Variation of the photosynthetic electron transfer rate and electron requirement for daily net carbon fixation in Ariake Bay, Japan

Y. Zhu [a], J.Ishizaka [b], S.C. Tripathy [c], S. Wang [d], Y. Mino [b], T. Matsuno [e], D.J. Suggett [f]

[a] Graduate School of Environmental Studies, Nagoya University, Nagoya 464-8601, Japan

[b] Institute for Space-Earth Environmental Research, Nagoya University, Nagoya 464-8601, Japan

[c] National Centre for Antarctic and Ocean Research, Earth System Science Organization, Ministry of Earth Sciences, Vasco-Da-Gama, Goa 403804, India

[d] School of Marine Sciences, Nanjing University of Information Science and Technology, Nanjing, 210044, Jiangsu, China

[e] Research Institute for Applied Mechanics, Kyushu University, Fukuoka, Japan

[f] Plant Functional Biology and Climate Change Cluster, University of Technology Sydney. P.O.Box 123, Broadway, NSW 2007, Australia

Accepted Journal of Oceanography in March 28, 2016

Abstract

Fast Repetition Rate fluorometry (FRRf) provides a potential means to examine marine primary productivity; however, FRRf-based productivity estimations require knowledge of the electron requirement (K) for Carbon (C) uptake (K_C) to scale an electron transfer rate (ETR) to CO_2 uptake rate. Most previous studies have derived K_C from parallel measurements of ETR and CO_2 uptake over relatively short incubations, with few from longer-term daily-integrated periods. Here we determined K_C by comparing depth-specific, daily ETRs and CO_2-uptake rates obtained from 24-h on-deck incubation experiments undertaken on seven cruises in Ariake Bay, Japan from 2008-2010. The purpose of this study was to determine the extent of variability of K_C and to what extent this variability could be reconciled with the prevailing environmental conditions, and ultimately develop a method for determining net primary productivity (NPP) based on FRRf measurements. Both daily ETR and K_C of upper layer varied considerably, from 0.5 to 115.7 mmol e^- mgChl-a^{-1} d^{-1} and 4.1 to 26.6 mol e^- (mol C)$^{-1}$, respectively, from throughout the entire dataset. Multivariate analysis revealed a strong correlation between daily photosynthetically active radiation (PAR) and K_C ($r^2 = 0.94$). A simple PAR-dependent relationship derived from the data set was used for generating K_C and this relationship was validated by comparing FRRf predicted NPP with ^{13}C uptake measured in 2007. These new observations demonstrate the potential application of FRRf for estimating regional NPP from ETR.

Keywords: FRR fluorometry; primary productivity; ETR; quantum requirement for carbon fixation; ^{13}C-uptake

1. Introduction

Fast Repetition Rate fluorometry (FRRf) non-destructively characterizes photosynthetic processes, including photosystem II (PSII) photochemistry and photosynthetic electron transport (Kolber et al., 1998). The technique has been widely considered a key milestone in aquatic research for global efforts to understand environmental regulation of primary productivity since the data can be acquired over unprecedented time and space scales, and with a resolution far beyond that from conventional incubation methods (Suggett et al., 2009a). While FRRf has been principally applied to phytoplankton studies examining effects of physiological stress, such as nutrient limitation (e.g. Behrenfeld and Kolber, 1999; Moore et al., 2006; Moore et al., 2008), it has also been utilized for characterisation light absorption (Suggett et al., 2004; Silsbe et al., 2015) and for interpreting phytoplankton photo-physiological processes in the context of phytoplankton community structure (Suggett et al., 2009b). The most attractive application is its potential for describing primary productivity (e.g. Suggett et al., 2001; Fujiki et al., 2008; Cheah et al., 2011). FRRf thus offers the potential for ground-truthing of remote sensing-based models for estimating primary productivity that are presently poorly resolved over time and space by conventional *in-situ* or simulated *in-situ* incubation CO_2 uptake experiments (Saba et al., 2011; Tripathy et al., 2012).

Determination of photosynthetic rate via FRRf differs from conventional CO_2-uptake (or O_2 evolution) measurements since it is derived from simultaneous measurements of light harvesting and utilization by photosystem II (PSII) (Kolber and Falkowski, 1993; Suggett et al., 2015) to yield PSII electron transfer rates (ETR, Oxborough et al., 2012). However, knowledge of the "quantum requirement for carbon fixation" ($\Phi_{e,C}$; Lawrenz et al., 2013, but recently termed K_C; Hancke et al.,

64 2015) is essential to convert the ETR to a biogeochemically meaningful measure of
65 primary productivity (Suggett et al. 2009a; Lawrenz et al., 2013; Hancke et al., 2015).
66 K_C implicitly accounts for various factors that decouple the ETR from CO_2
67 uptake, notably cellular processes other than CO_2 assimilation that consume energy
68 and reductant (e.g. Suggett et al., 2009a). However, since K_C is determined from
69 parallel measurements of ETR and CO_2 uptake, it also accounts for methodological
70 limitations inherent to estimating the ETR (Schuback et al., 2015) and CO_2 uptake
71 (Kromkamp et al., 2008; Lawrenz et al., 2013). Even so, such 'conversion factors'
72 appear generally robust since they can be modeled as a function of key environmental
73 drivers across local to regional scales (Lawrenz et al., 2013; Schuback et al., 2015).
74 Lawrenz et al. (2013) synthesized available global FRRf-based K_C estimates to
75 demonstrate that K_C could be frequently predicted as a function of key environmental
76 factors controlling primary productivity, i.e. light, temperature and inorganic nutrient
77 availability, albeit with large spatial variability. Whilst the reason underpinning this
78 variability still remains unclear, it likely reflects localized differences in physiological
79 conditions regulated by specific phytoplankton communities and their environmental
80 conditions. Indeed recent efforts of sampling across broad iron-limited regions of the
81 northeast subarctic Pacific indicate that K_C is highly predictable and the estimation
82 can in fact be achieved from other FRRf-based physiological proxies, such as
83 non-photochemical quenching (Schuback et al., 2015).
84 Despite the increasing use of FRRf within the coastal waters of Japan, there have
85 been no focused studies aimed at understanding the variability of K_C and its regulation
86 by environmental factors. Here we report new data describing the variability of K_C
87 from a semi-enclosed bay, Ariake Bay, Japan. This study location (Fig. 1) offered us
88 the opportunity for repeated sampling under a range of environmental conditions.

Ariake Bay is nutrient rich and considered a highly productive ecosystem (Ishizaka et al., 2006). Previous studies in this bay by Tripathy et al. (2010, 2012) provided strong indications that the FRRf might be a powerful tool for estimating primary productivity in this area, but was limited by the need to assume K_C. Here we propose a new FRRf-based approach for examining K_C for this region by comparing daily-integrated ^{13}C-uptake rates (and hence net primary productivity) with corresponding measurements of daily-integrated ETRs. The main objectives of this study are three fold: first to determine the extent of variability of K_C; second, to evaluate the environmental factors responsible for this variability and third, to establish an FRRf based approach for *in situ* net primary productivity (NPP) estimation.

2. Materials and Methods

2.1. Sample collection, processing and analyses

The sampling protocols utilized in our study are similar to those reported in Tripathy et al. (2010; 2012) and Shibata et al. (2010). In brief, the core observations were from 7 cruises in Ariake Bay (Fig. 1) during fall/spring seasons of 2008, 2009 and 2010 (Table 1). An additional sampling campaign from December 2007 was used for later validation of our FRRf-NPP prediction model. For all cruises, seawater samples were collected at a fixed station "T1" (130.31° E, 32.91° N, Fig. 1) from 6 discrete depths (corresponding to ca. 1%, 5%, 10%, 25%, 50% and 100% of Photosynthetically Active Radiation, PAR, 400-700 nm, at the sea surface) using a rosette sampler equipped with twelve 5 L Niskin bottles (General Oceanics) and a conductivity-temperature-depth profiler (CTD, 911+, SeaBird Electronics). Data from the CTD was utilized for establishing hydrographic conditions at St. T1 at the time of

sampling. For 24 h on-deck ^{13}C uptake incubations, and for Chl-a, nutrient and phytoplankton spectral light absorption measurements, water samples were taken from pre-dawn CTD casts. All seawater samples were first carefully drained from the Niskin bottles into appropriate incubation and/or sampling bottles and further processed as described below.

Chl-a concentrations were determined from 100 ml seawater samples filtered onto 25 mm glass fiber filters (Whatman GF/F) under low vacuum (<0.02 MPa). Filters were then extracted in N, N-dimethylformamide for 24 hours in darkness (Suzuki and Ishimaru, 1990) and Chl-a quantified using a pre-calibrated fluorometer (10-AU, Turner Design). Samples for nitrate + nitrite, phosphate and silicate analyses were stored at -20 ℃ until later analysis using an automated nutrient analyzer (AACS-IV, BLTEC).

Phytoplankton absorption coefficients, $a_{ph}(\lambda)$ (m^{-1}), were determined using the quantitative filter technique of Kishino et al. (1985) as adapted by Wang et al. (2014). 250 ml seawater samples were carefully filtered through Whatman GF/F (25 mm) to ensure even distribution of the particulate matter on the filters. The optical density (OD) of all particulate components were measured in a dual beam multi-purpose spectrophotometer (MPS-2400, Shimadzu Inc.) over wavelengths from 350 to 750 nm at 1-nm intervals, before and after the extraction of phytoplankton pigments by methanol. The absorption spectra of particulate material obtained after pigment extraction is that of non-phytoplankton particles. The spectral absorption coefficients of total particulate material ($a_p(\lambda)$) and non-phytoplankton particles and ($a_{np}(\lambda)$), respectively) were determined using the equation $2.303 \cdot OD(\lambda) \cdot S/V$, where 2.303 is the factor used to convert common to natural logarithm, S is the filter clearance area (m^2), and V is the volume of sample water filtered (m^3). Phytoplankton specific

absorption spectra ($a_{ph}(\lambda)$) were then obtained by subtracting the non-phytoplankton absorption from total absorption as,

$$a_{ph}(\lambda) = a_p(\lambda) - a_{nph}(\lambda) \quad (1)$$

Chl-a specific absorption coefficient, $a^*_{ph}(\lambda)$ (m^2 mg Chl-a $^{-1}$), was then calculated by standardizing $a_{ph}(\lambda)$ by Chl-a concentration.

2.2. ^{13}C uptake based net primary productivity estimates

^{13}C uptake experiments were carried out via 24 h on-deck simulated-in-situ (SIS) incubations with enrichment of ^{13}C stable isotope (min 98 atom%; $NaH^{13}CO_3$, ISOTEC), where the final ^{13}C atom % of total dissolved inorganic carbon was ca. 10% of that in the ambient water (Hama et al., 1983). ^{13}C labelled sodium bicarbonate was added to each of quadruplicate 1 L bottles containing seawater from each light depth sampled; three of the replicates were then immediately transferred to incubators in which light was attenuated with blue plastic filters (The General Environmental Technos), and the fourth replicate filtered immediately to serve as the time zero, and adsorption correction of the ^{13}C label on to the filters. The use of blue filters in the incubators simulated *in-situ* irradiance spectra at depths consistent with sample collection. Incubators were set up with a continuous flow-through system of surface seawater to maintain ambient temperatures. We acknowledge that differences between incubation and *in situ* temperatures for deeper samples may raise errors for carbon uptake rates; however, these errors should not be significant in this study since temperature differences between surface and Z_{eu} were less than 0.7 ℃ across all cruises (Davison, 1991).

All samples were filtered through 25mm pre-combusted GF/F filters (450 ℃, 4 hours) and stored at -20 ℃ until further analysis. The filter samples were vacuum

dried after exposure to fumes of HCl to remove excess inorganic particulate carbon. The concentration of particulate organic carbon (POC) and the isotopic ratio of ^{13}C and ^{12}C (^{13}C atomic %) on the filters were then determined by isotope ratio mass spectrometer (Delta^{PLUS}, Thermo Fisher Scientific) equipped with an elemental analyzer (EA 1110, CE Instruments). Carbon fixation rates (PP) were calculated according to Hama et al. (1983). Chl-a concentrations before and after the incubation were measured to examine for any drift during the incubations; Chl-a decreased significantly (from ca. 4.43 to 2.28 mg m^{-3}) between the start and end of the incubation period from the cruise on the 14 May, 2010, and so the primary production data from this cruise were excluded from all further analysis. Chl-a specific primary productivity (P^B) was PP divided by Chl-a concentration, and the water column integrated PP (IPP) was defined as $\int_0^{Zeu} PP(z)dz$.

2.3 *in-situ* PAR and irradiance spectrum measurements

Underwater PAR was quantified using a scalar sensor (QSP-200L and QSP-2200, Biospherical Inc.) attached to both the CTD and FRRf frames, and these datasets were both used to subsequently determine the diffuse attenuation coefficient for PAR, $K_d(z)$ (m^{-1}). Incident PAR at the sea surface ($PAR(0^+)$) was measured throughout the incubation period using a quantum scalar irradiance sensor (QSL-2100, Biospherical Inc.) mounted on the incubators used for ^{13}C uptake experiments. The *in situ* underwater irradiance field $E_d^-(\lambda, z)$ was measured by an underwater spectral radiometer (PRR-800, Biospherical Instruments) at 13 wavelengths (λ = 380, 412, 443, 465, 490, 510, 532, 555, 565, 589, 625, 665 and 683 nm) every 2 hours from 8:00-16:00 (local time).

2.4. FRRf parameters, electron transport rate (ETR) and K_C

Daily time series of active Chl-a fluorescence profiles were measured every 2 hours from dawn until dusk (Table 1) from the near surface to depths of ca. 20 m in the water column using a Diving Flash FRRf (Kimoto Electric). The profiling speed was set to < 0.2 m s^{-1} to ensure acquisition of fine scale vertically resolved active fluorescence data (Mino et al., 2014). The Diving Flash is designed to measure fluorescence simultaneously in a "dark" chamber, which is fully shaded, and in a "light" chamber equipped with a dichroic cyan filter to reduce the probable influence of red light effect (Raateoja et al., 2004; Tripathy et al. 2010). The FRRf uses a single-turnover protocol and was programmed to deliver sequences of 60 saturation blue flashlets (wavelength of 470 nm with a 25 nm half bandwidth, each 2 µs in duration at 4 µs intervals), followed by 20 relaxation blue flashlets (each 2 µs in duration at 75 µs intervals) (as per Fujiki et al., 2008). Fluorescence parameters derived from both dark (F_o, F_m, σ_{PSII} and F_v/F_m) and light (F', F_m', σ_{PSII}' and F_q'/F_m') chambers (refer to Table 2) were calculated using the software (FRRCalc2, Kimoto). Calculation was based on the KPF model fits to FFRf induction curves to resolve physiological parameters (Kolber et al., 1998). Inter-calibration of dark and light chambers was undertaken based on the F_m correction from pre-dawn casts.

Measurements of the effective absorption cross section (σ_{PSII}) were weighted to the narrow blue excitation waveband of the FRRf light source (470 nm) and therefore were adjusted to the spectra of the *in situ* irradiance following Suggett et al. (2006b) as:

$$\sigma_{PSII}^{abs} = \left(\frac{\bar{a}^{chl}(in\ situ)}{\bar{a}^{chl}(FRRf)}\right) \times \sigma_{PSII}, \quad (2)$$

where $\bar{a}^{chl}(FRRf)$ and $\bar{a}^{chl}(in\ situ)$ represent the absorption coefficients from

Eq.(1) weighted to the incident spectra of the FRRf's excitation (Suggett et al., 2004) and *in situ* irradiance, respectively. $\bar{a}^{chl}(FRRf)$ and $\bar{a}^{chl}(in\ situ)$ were calculated from $\bar{a}^{chl} = \sum([a^{chl}(\lambda) \times E(\lambda)]/\sum[E(\lambda)])$, where E refers to the irradiance spectrum of either the FRRf excitation LED or *in situ* light field (see Suggett et al., 2001). The spectral range λ of $\bar{a}^{chl}(FRRf)$ and $\bar{a}^{chl}(in\ situ)$, 400 – 700 nm, was assessed at 1 nm intervals and therefore 1nm resolved *in situ* light fields were generated by interpolating between the discrete wavebands of the PRR800 (Suggett et al., 2001).

Absolute electron transfer rate (ETR, mmol e^- (mg Chl-a)$^{-1}$ h^{-1}) were then determined following Suggett et al. (2009a) as follows:

$$\mathrm{ETR} = \mathrm{PAR} \times \sigma_{PSII}^{abs} \times n_{PSII} \times q_p \times 0.0243, \quad (3)$$

where PAR is in units of μmol quanta m^{-2} s^{-1}, σ_{PSII}^{abs} is the spectrally corrected effective absorption cross section of PSII from the dark chamber ($Å^2$ $quanta^{-1}$), and n_{PSII} is the ratio of functional PSII reaction centres to Chl-a (mol RCII (mol Chl-a)$^{-1}$). q_p (or Fq'/Fv') is the photochemical quenching coefficient under actinic light estimated as the difference of apparent PSII photochemical efficiencies measured in 'light' and 'dark' chambers of the FRRf (see Table 2), following the procedure of Suggett et al. (2006a,b, 2011). The factor 0.0243 converts seconds to hours, μmol quanta to mol quanta, $Å^2$ to m^2 and mol Chl-a to mg Chl-a. Following Kolber and Falkowski (1993), n_{PSII} was assumed to be a constant i.e. 0.002 mol RCII mol Chl-a^{-1} since the phytoplankton populations we examined were mostly dominated by eukaryotes, mainly diatoms, *Skeletonema spp*., and dinoflagellates, *Ceratium furca* (Shibata et al., 2010). It may be noted that assigning a constant value to n_{PSII} has been recognised as a potential source of error to ETR determinations (e.g. Suggett et

al. 2004, 2009b, 2011), which we discuss later.

Previous work has shown that differences between ^{13}C-based CO_2 uptake rates and FRRf-based *in situ* ETRs appear to predominantly reflect differences in light fields in the two measurements (Tripathy et al., 2010). Thus, in order to account for high frequency fluctuations in the incident irradiance field between the FRRf casts (every 2 hours), a simple modelling approach was utilized to estimate daily-integrated ETR, which was subsequently used for comparison against daily-integrated ^{13}C uptake rates. Our approach is analogous to those previously used for determining daily ETR (Suggett et al. 2001, Smyth et al. 2004, Mino et al., 2014).

We determined ETR versus PAR relationships for each light depth corresponding to the 6 sample depths of the ^{13}C uptake experiments (100, 50, 25, 10, 5 and 1% of the PAR(0^-). Incident PAR logged continuously at the surface was multiplied by the factor 0.9 to account for physical properties at the air-sea interface which reduce PAR above the water surface, PAR(0^+), relative to that just beneath the surface, and PAR(0^-) (Marra, 2015). Underwater PAR at the % light depth of interest (x%) was then determined as PAR(0^-)(t) $\times$ (x/100).

ETR versus instantaneous PAR relationships were constructed for each cruise using data from the FRRf time series casts, and the model of Jassby and Platt (1976), to determine α and ETR_{max} which are two fitted parameters describing the initial slope of the ETR vs PAR curve and the maximum electron transfer rate,

$$ETR(z,t) = ETR_{max} \times \tanh(\frac{\alpha PAR(z,t)}{ETR_{max}}), \quad (4)$$

.

With knowledge of α and ETR_{max}, we were then able to retrieve the ETR for any given value of PAR from the continuous underwater light field and thus determine

the daily integrated ETR at specific depth, according to following equation:

$$ETR\_daily(z) = \int_{t1}^{t2} ETR(z,t)dt, \quad (5)$$

where the period between t1and t2 represent the time in hours from dawn to dusk.

Finally, the electron requirement of carbon uptake K_C (mol e^- (mol C)$^{-1}$) was calculated as,

$$K_C = ETR\_\text{daily}/P^B \times 12 \ , \quad (6)$$

where ETR_daily (mol e^- mg Chl-a^{-1} d^{-1}) and P^B (mgC mg Chl-a^{-1} d^{-1}) were the daily-integrated ETR and daily-integrated carbon assimilation per unit Chl-a, and the factor 12 converts g C to mol C.

In addition to determining ETR, FRRf casts were also used to determine a proxy for non-photochemical quenching (NPQ), so as to verify recent observations as to whether K_C (under conditions where n_{PSII} is unknown and hence an assumed constant) was closely related to the extent of NPQ (Schuback et al., 2015). Specifically, the photochemical efficiency measured in the dark chamber for any given depth, $F_v/F_m(z)$, was normalised to the maximum photochemical efficiency measured throughout the water column (Suggett et al., 2006b; 2011); this maximum typically occurs at low light depths where the influence of surface-driven NPQ is eliminated and hence corresponds to the dark-acclimated maximum efficiency $(F_v/F_m)_M$ (Smyth et al., 2004; Suggett et al. 2011). Thus our NPQ Proxy (NPQ*) (z) = 1- $[F_v/F_m(z) / (F_v/F_m)_M]$. In order to compare NPQ* with the daily K_C for each light depth, we determined the daily mean NPQ* (z) from across all casts throughout the day.

2.5 Statistical analyses

Spearman Rank Order Correlation analysis was used to evaluate the key environmental variables that may be related with K_C. Correlations were considered significant when p was < 0.05. Stepwise Multiple Regression (SMR) was then utilized to generate the model for estimating the dependent variable (i.e. K_C) from the various independent variables (i.e. environmental factors). p-values (< 0.05) from the SMR were used as the criterion for choosing environmental variables entered into the K_C prediction model. The Spearman Rank Order Correlation Analyses and SMR were performed using open source statistical software R version 3.1.0 (R Core Team 2014).

3. Results

3.1 Physicochemical characteristics and phytoplankton biomass

Cruises were conducted in fall November 2008 and 2009 and in spring May 2008 and 2010. Water column properties during the two seasons when these cruises were undertaken were quite different (Table 1, Fig. 2). Vertical profiles of PAR, temperature, salinity, and density plotted for each cruise (Fig. 2), revealed higher daily PAR, lower temperature and lower surface salinity during May as compared to Nov (Fig. 2a-c). Mixed layer depth, defined as depth at which the density change from the surface density was 0.03 kg m^{-3} (Shibata et al., 2010), generally showed deeper mixing in Nov than May (Table 1, Fig. 2d). Surface PAR values were higher in May; however, the average euphotic depth, Z_{eu}, and average diffuse attenuation coefficient, K_d, generally similar for the two seasons (May, 13.5 ± 1.9 m, 0.33 ± 0.04 m^{-1}; November, 16.3 ± 3.2 m, 0.29 ± 0.07 m^{-1}). Thus similar vertical attenuation of light in the water column was evident for both seasons.

Average inorganic nutrient concentrations, $NO_3^-+NO_2^-$, PO_4^{3-} and SiO_2 were 13.8 ± 0.6, 1.34 ± 0.04 and 57 ± 3 μM, respectively in November, and generally constant throughout the mixed water column (Fig. 3a,b,c) as expected given the uniform profiles of density with depth (Fig. 2d). $NO_3^-+NO_2^-$ and PO_4^{3-} concentrations were lower in May than for November (0.4 ± 0.1 and 0.16 ± 0.06 μM). The ratio of $NO_3^-+NO_2^-$ and PO_4^{3-} concentrations (N/P ratio) was < 5 across all depths in May but increased significantly in November, and with mean value of 10.2 (Fig. 3d). Chl-a concentrations were generally similar across all depths and consistently lower in May (1.18-3.87 mg m^{-3}) than in November (1.92-6.61 mg m^{-3}) except in 15 Nov 2009 (Fig. 3e).

3.2 Variability of FRRf parameters and ETR

Time series profiles of FRRf derived photo-physiological parameters obtained throughout the day on 21 May 2010 (hereafter referred to as May) and 8 November 2008 (hereafter November) are presented in Figs. 4a-d and Figs. 4e-h respectively. The FRRf data from these two cruises are taken as representative profiles associated with the differences in hydrographical and climatic conditions during the two seasons (shallow vs. deep mixed layer; high vs. low daily PAR).

In May, the ratio for σ_{PSII} spectral weighting, $\bar{a}^{chl}(in\ situ)\ :\ \bar{a}^{chl}(FRR)$ varied from 0.60 at surface to 0.49 at 1% PAR depth, with mean 0.54 ± 0.04 (Fig. 5). Considering this small vertical variation, we used the mean value for correcting σ_{PSII} across all depths. σ_{PSII}^{abs} values plotted after this correction varied over depth and time, from 248 to 386 $Å^2$ $quanta^{-1}$, and a mean value of 334 ± 30 $Å^2$ $quanta^{-1}$ (Fig. 4a). σ_{PSII}^{abs} values increased with depth, from the surface to ca. 8 m depth (10% surface PAR depth), at which point they appeared to plateau and attain relatively constant values in the deeper layer. Over the course of the day, maximum and minimum values of near surface σ_{PSII}^{abs} were observed at 6:00 and 10:00 cast, respectively. The mean σ_{PSII}^{abs} of the upper layer (from the surface to 10% PAR depth) was calculated to be 303 ± 35 $Å^2$ $quanta^{-1}$. In November, $\bar{a}^{chl}(in\ situ)\ :\ \bar{a}^{chl}(FRR)$ was slightly larger than that observed in May, with a mean value 0.64 ± 0.03 (0.69 to 0.58; Fig. 5). After applying this spectral correction, σ_{PSII}^{abs} varied from only 296 to 403 $Å^2$ $quanta^{-1}$, and with a higher mean value of 360 ± 23 $Å^2$ $quanta^{-1}$ indicative of low light acclimation (Moore et al., 2006). As observed in May, σ_{PSII}^{abs} values increased with depth, but the difference in σ_{PSII}^{abs} values throughout the water column was smaller in November than May (Fig. 4a, e).

Values of the maximum photochemical efficiency, F_v/F_m (dimensionless) were relatively similar for both cruises, ranging 0.31-0.52 in May and 0.36-0.54 in November, respectively. Below 10% PAR depth (8m) variation of F_v/F_m over the course of the day was generally low compared to that at the surface. The reduced values of F_v/F_m in the upper layer during the day can be attributed to the NPQ (Suggett et al., 2011) (Fig. 4b, f). Values for q_p during both cruises were close to the maximum of 1 at depths > 10 m and lowest at the surface (Fig. 4c, g). Surface values of q_p were lower (0.5) in May as compared to 0.64 in November. These differences in photochemical quenching reflect differences in surface irradiances in May and in November.

Changes in ETR over the course of the day reflected the variations in ambient PAR, σ_{PSII}^{abs} and q_p (Table 3). The large changes in ETR values at depths < 10 m during the May cruise are from the larger differences in σ_{PSII}^{abs} and q_p during May. Vertical profiles of ETR values maintained a consistent trend with depth (and at depths shallower than 10 m differed appreciably over the course of the day) throughout, but maximum values in May were almost twice as that in November (Fig. 4d, h).

Light response models applied to ETR versus PAR scatter plots for all seven cruises are shown in Figs. 6a-g, and the fitted parameters presented in Table 4; these parameters were then utilized to derive the daily ETR based on Eq. 5 (Fig. 7a). Daily ETR calculated from all pooled data and plotted versus optical depths varied considerably, from 0.5 to 115.7 mmol e^- (mg Chl-a)$^{-1}$ d^{-1}, resulting in an average (± standard deviation) of 24.8 ± 27.5 mmol e^- (mg Chl-a)$^{-1}$ d^{-1} (Fig. 7a). The daily ETR of upper lit layer (> 10% PAR depth) averaged 60.4 ± 29.9 mmol e^- (mg Chl-a)$^{-1}$ d^{-1}, n=18) in May and was almost twice of the ETR observed in November, 33.6 ± 17.3

370 mmol e^- (mg Chl-a)$^{-1}$ d^{-1}, n=24). For all cruises, ETR increased progressively from
371 deeper to shallower optical depths. The relationship between daily ETR and PAR
372 plotted in Fig. 7b shows a significant correlation (r^2=0.98, n=42, $p < 0.001$) between
373 these two parameters, with fitted maximum ETR of ca. 120 mmol e^- (mg Chl-a)$^{-1}$ d^{-1}.

374 **3.3 Carbon uptake rates**

375 Daily Chl-a normalised carbon uptake rates (P^B) varied from 2.95 to 69.9 mgC mg
376 Chl-a^{-1} d^{-1}, with an average value of 31.65±17.09 mgC mg Chl-a^{-1} d^{-1}. Profiles of P^B
377 plotted in Fig. 8a showed signs of photoinhibition during several cruises, which was
378 not consistent with the profiles of daily ETRs in which no subsurface maximum was
379 observed. Differences in the highest and lowest P^B for the two seasons were also small
380 (69.9 and 2.95 mgC mg Chl-a^{-1} d^{-1} in May; 58.47 and 3.36 mgC mg Chl-a^{-1} d^{-1} in
381 Nov.). Amongst all cruises, the mean value of P^B_{opt} (defined as the maximum P^B
382 within the water column) in May, 62.7 mgC mg Chl-a^{-1} d^{-1}, was larger than that for
383 November, 47.0 mgC mg Chl-a^{-1} d^{-1}.

384 P^B values were plotted against corresponding ETR values (Fig. 8b) to examine the
385 extent with which water column primary productivity values can be explained by ETR.
386 Overall, values of P^B and ETR generally co-varied well for lower ETR values.
387 However, when daily ETR values exceeded ca. 20 mmol e^- [mgChl-a]$^{-1}$ d^{-1}, relatively
388 large variations between P^B and ETR were observed suggesting that beyond a certain
389 threshold, measurements of daily ETR cannot adequately reflect carbon fixation rates.

390 **3.4 Variability of the quantum requirement (K_C)**

391 One of our goals was to examine whether the breakdown of the relationship
392 between ETR and P^B could be explained by changes in values of K_C over the course
393 of the day or with depth. Values of K_C determined from corresponding values of daily

ETR and C-uptake (Eq. 6) exhibited a range of 2.3-26.6 mol e^- (mol C)$^{-1}$ in May (mean ± standard deviation: 13.2 ± 17.9 mol e^- (mol C)$^{-1}$) and 1.2-19.3 mol e^- (mol C)$^{-1}$ in November (mean: 5.7 ± 4.7 mol e^- (mol C)$^{-1}$), and were always higher for surface than deep waters (Fig. 9a).

K_C values at higher optical depths (i.e. 1% and 5% of PAR at the surface, roughly < 3 mol quanta m^{-2} d^{-1}) recorded during our study were lower than the theoretical minimum value of 4 mol e^- (mol C)$^{-1}$. Since the shallower optical depths (shallower than the 10% PAR depth) contribute to ~80% of water column integrated NPP (IPP) in our study area, we therefore excluded K_C values where daily PAR < 3 mol quanta m^{-2} d^{-1} from further analysis. With the exclusion of this data, K_C varied from 4.1 to 26.6 mol e^- (mol C)$^{-1}$ (Fig. 9b).

Variability of K_C was finally examined in the context of the prevailing environmental variables using Spearman Rank Oder Correlation analysis. SMR analysis was further used to establish the relationship between the key environmental regulators of K_C ($p < 0.05$). These analyses revealed that K_C was highly related to incident irradiance ($r^2 = 0.941$, $p < 0.001$; Table 5). SMR provided the best model fit for predicting K_C on the basis of PAR (Fig. 9c). Using the same analytical steps we were further observed a significant correlation between K_C and non-photochemical quenching (NPQ*) (Fig. 9d).

4. Discussion

Previous FRRf-based observations in Araike Bay study (Tripathy et al. 2010) relied on a constant value (= 4) for K_C for estimating daily photosynthetic rates and subsequent comparison with carbon uptake measurements from ^{13}C incubation experiments; this work demonstrated reasonably good agreement between FRRf and

C uptake based primary productivity when ambient light intensities were low. However, Tripathy et al. (2010) considered that the FRRf method overestimated daily net primary production two to three fold in particular at the surface (i.e. under high light conditions) and hypothesised that the assumed constant K_C likely led to significant errors in FRRf-based primary productivity estimates, especially when light intensities are high. Our current study has directly addressed and confirmed this hypothesis. Specifically, we show for the first time that the electron requirement for net carbon fixation (K_C) varies in a predicable manner with the daily irradiance. These observations are consistent with recent reports suggesting that K_C is highly variable but can potentially be predicted from knowledge of key environmental variables (Lawrenz et al., 2013). In the following sections, we consider our results that net primary production can be estimated by FRRf directly when light-dependent variability in K_C is accounted for in the eutrophic enclosed bay, Ariake Bay.

4.1 Reconciliation of ETRs and ^{13}C uptake rates

Values of K_C from the upper layer in our study varied from 4.1 to 26.6 mol e^- (mol C)$^{-1}$, with a mean and standard deviation of 9.6 ± 5.4 mol e^- (mol C)$^{-1}$. These values are within the range of 1.15-54.2 (mean: 10.9 ± 6.91) mol e^- (mol C)$^{-1}$ global observations of K_C (Lawrenz et al. 2013), which were derived in large part from short-term incubations, typically 1-4 h. In principal K_C should increase as C-uptake increasingly transitions from gross to net (e.g. Halsey et al. 2013); thus, the general agreement of our mean K_C values to those previously measured elsewhere (Lawrenz et al. 2013) would suggest net carbon uptake rates may already be attained after relatively short incubations. However, our higher values are generally more consistent with those measured under conditions of nutrient stress and/or limitation, which

442 elevates K_C (Lawrenz et al. 2013). Since our study did not appear to be under the
443 influence of nutrient stress the higher values we observed could indeed reflect
444 'inflation' from a prolonged incubation period of net carbon uptake. Unfortunately it
445 is presently impossible to reconcile the confounding influence of incubation length
446 and the broad variation that appears evident for K_C across studies/regions, and thus
447 warrants further attention.

448 In previous FRRf-based studies (Corno et al. 2006; Melrose et al. 2006; Suggett
449 et al. 2006a; 2009a), values for K_C lower than the theoretical minimum (i.e. 4 mol e^-
450 (mol C)$^{-1}$) have often been measured but still hard to resolve. In fact the long
451 incubation times during SIS experiments generally yield CO_2 uptake closer to net
452 primary production (Marra, 2009), and thus increases the expected minimum value for
453 K_C. Specifically, net CO_2 uptake rates are typically lower than gross uptake rates by a
454 factor of ca. 6-55%, depending on respiration loss of different phytoplankton species
455 and their growth phase (López-Sandoval et al., 2014). This suggests the minimum
456 value for K_C under net carbon uptake conditions should ultimately be considered
457 higher than 4 mol e^- [mol C]$^{-1}$. When all sample depths were considered in our study,
458 values of K_C < 4 mol e^- (mol C)$^{-1}$ contributed ca. 40% of the total number of samples.

459 K_C values below the 'theoretical minimum' are generally considered an
460 overestimation of carbon uptake and/or underestimation of ETR (Suggett et al., 2009a;
461 Lawrenz et al. 2013). Therefore we further analysed our data set excluding values of
462 K_C from deeper waters (where values < 4 mol e^- (mol C)$^{-1}$, were observed) with the
463 justification that net primary productivity at these depths generally contribute a very
464 small fraction of integrated euphotic water column net primary production. In this
465 way we were able to generate a clear positive correlation between upper layer K_C and
466 daily irradiance (and with the intercept of the regression close to the theoretical

minimum for K_C. Even so, greater understanding of why values for K_C often drift < a value of 4 requires more focused study in future. Several potential variables can contribute to potentially erroneous ETRs (see Suggett et al. 2009a). Our ETR calculation (Eq. 3) assumed a 'standard' n_{PSII} value of 0.002 mol RCII [mol chl]$^{-1}$ for eukaryotes (Kolber & Falkowski 1993) since phytoplankton in this region were mainly dominated by diatoms and dinoflagellates during the two study seasons (Shibata et al., 2010; Tripathy et al., 2010). Suggett et al. (2011) reported a mean n_{PSII} of 0.00188 ± 0.00002 mol RCII [mol Chl-a]$^{-1}$ for 2 and 7 species of dinoflagellates and diatoms under various growth conditions. Thus, the observations of Suggett et al. (2011) suggest that our use of constant n_{PSII} would potentially lead to very small errors in the estimation of K_C. Our values for σ_{PSII} was spectrally corrected, and 'sample blanks' not required based on our approach to estimate qP (Suggett et al. 2006a, b) and therefore also unlikely contributed a major course of error in our ETRs.

4.2 Decoupling of ETR from carbon uptake

Our study shows that the decoupling of ETR from 24-h net C-uptake was most significant at higher irradiances, a finding that is consistent with the observations of Schuback et al. (2015) across a broad range of biogeographic areas, with shorter incubation time (3-4 hours). Light-dependency of K_C has been reported for microalgae, and generally higher values of K_C have been recorded under light-saturated conditions (Suggett et al., 2008; Brading et al., 2013; Hancke et al., 2015). High ETRs can be sustained through up-regulation of alternative electron flow pathways (Prasil et al., 1996; Mcdonald et al., 2011) and/or light-dependent O_2 consuming processes (Suggett et al. 2008; Mackey et al. 2008). Such processes, which include Mehler Ascorbate Peroxidase and plastoquinone terminal oxidase (PTOX) activity, act to balance the availability of light energy with the amount of reductant in cells when rates of linear electron transport exceed the capacity for CO_2 assimilation (e.g. Cardol et al., 2011).

The relationship between K_C and light availability may further explain why we also observed co-variability of K_C with the inherent NPQ capacity (Fig. 8d), observations that are again consistent with those of Schuback et al (2015) but form iron-limited waters. Sustained electron transport activity under high light and hence ΔpH-triggering NPQ has been reported previously for both diatoms and dinoflagellates (Ott et al., 1999; Lavaud et al., 2004), i.e. groups that generally dominate Ariake Bay (see above). It is known that NPQ shows predictable light-depenency dynamics as a result of energy-dependent quenching in the light harevting antennae (e.g. Serodio & Lavaud 2011). So clearly excess light would also increase the NPQ expression and explain the linear relation between K_C and NPQ* observed here.

506 Despite the observed light regulation of K_C in our study, we cannot fully exclude
507 the potential effects of other factors that could co-vary with light availability (Table 5).
508 Specifically, the highest values of K_C corresponded to the lowest $NO_3^-+NO_2^-$ and
509 PO_4^{3-} concentrations found in the upper stratified waters in May, i.e. when light
510 intensity was also high. Previous comparison studies between ETR and C-uptake
511 clearly show variability of Kc was correlated to that of temperature and/or inorganic
512 nutrients rather than light availability in some biogeographic regions (see Lawrenz et
513 al, 2013). Such environmental factors also drive large changes in both phytoplankton
514 community structure and physiological status , both of which can drive variance in K_C
515 (Debes et al., 2008; Kromkamp et al., 2008; Suggett et al., 2006b, 2009a; Robinson et
516 al., 2014).
517 To evaluate for potential effects of nutrient concentrations on K_C, we compared
518 values for K_C from two cruises (28 May, 2008 vs. 08 Nov., 2008) from days with
519 similar daily light intensity (ca. 19 vs. 15 mol quanta m^{-2} d^{-1}) but with large
520 differences in nutrient concentrations (average $NO_3^-+NO_2^-$: 0.4 vs. 14.5 μM; PO_4^{3-}:
521 0.22 vs. 1.18 μM). Despite differences in nutrient conditions for these two cruises, the
522 K_C values were similar i.e. 7.9 ± 2.4 mol e^- (mol C)$^{-1}$ for May 28, 2008 as compared
523 to 8.5 ± 1.8 mol e^- (mol C)$^{-1}$ for November 06 2008. Thus, any influence upon K_C
524 from nutrients is likely secondary to that from light in our study area. Nitrogen is
525 considered to be limited in May (N/P: ca. 2.6), and appeared relatively low
526 concentration in water column (0.16 – 0.84 μM); however it should be noted that our
527 nitrogen data does not include ammonium-nitrogen (NH_4^+-N), which may account for
528 ca. 30% of the total DIN amount (Tabata et al., 2015). Thus it is unlikely nutrient
529 stress is significant even in May in Araike Bay. Comparable measurements of F_v/F_m
530 for May and November further suggest a lack of major nutrient stress (but see Suggett

et al. 2009b). This absence of nutrient stress probably explains why we were not able to observe a robust relationship between nutrients and K_C.

Our results suggest that in the Ariake Bay, where land-derived nutrient inputs are large, phytoplankton rarely experience nutrient starvation. Under these conditions, incident PAR appears the main factor responsible for the variability in K_C. This result contrasts with that of Lawrenz et al. (2013), where variance of K_C appeared more commonly governed by that of temperature, nutrients and/or light attenuation. However, this may reflect a lower range of temperature and nutrients (and Chl-a) observed across our dataset relative to the variance in K_C measured. Furthermore, Lawrenz et al. (2013) do not consider absolute PAR as a variable only K_d and optical depth within their meta-analysis, thus it is impossible to verify how local light conditions at the time of sampling may potentially have further contributed to the variability they observed. We have shown that K_C can be estimated by a simple light dependence from easily measurable irradiance in this region. Whether the resulting regression may perhaps be applicable to the other locations with similar environmental characteristics (i.e. absence of nutrient limitations and/or homogenous distribution of phytoplankton groups) remains to be seen.

4.3 Recommendations for future *in situ* application

The final objective of this study was to estimate NPP from FRRf directly. We have demonstrated that the key factor (K_C) for converting FRRf based ETR values to NPP can be derived from light intensity. The ETR vs. PAR relationship from FRRf deployments around noon when instantaneous PAR was highest, combined with continual surface PAR records, could be applied for regional estimates of NPP estimation. The advantage here of active fluorometry is that a large amount of *in situ*

555 data covering broad spatial (and temporal) scales can be acquired, which in turn can
556 further be utilized for validation of NPP derived from satellite data (as in Behrenfeld
557 et al., 1997; Kameda and Ishizaka, 2005; Hirawake et al., 2012). Before this becomes
558 a real possibility, several issues must first be addressed:

559 Firstly, the need for additional spectrally-resolved absorption and in-water
560 irradiance measurements to spectrally correct σ_{PSII}. Suggett et al. (2006b) previously
561 overcame this problem for FRRf data collected across many water types using an
562 algorithm between the spectral correction factor and optical depth. For our study, we
563 observed reactively little variability of the correcting factor for σ_{PSII}, and therefore
564 for practical reasons used a constant value for each season (i.e. 0.54 in spring/summer
565 and 0.64 in fall/winter; and thus an overall average value (i.e. 0.6) for σ_{PSII}. This
566 approach clearly simplifies broad-scale deployment of the FRRf but requires further
567 verification.

568 Secondly, it is not possible to measure n_{PSII} in most natural samples but some
569 knowledge of the RCII concentration can be obtained indirectly (Suggett et al., 2011)
570 or through new algorithms for calibrating [RCII] from the FRRf parameters
571 themselves (see Oxborough et al. 2012). In the semi-enclosed water region as Ariake
572 Bay or estuary, where nutrient concentrations remain relatively high and the
573 phytoplankton community dominated by micro-phytoplankton, n_{PSII} was considered
574 to remain at a constant value of 0.002 mol RCII (mol Chl-*a*)$^{-1}$ but again ultimately
575 requires further verification. Furthermore, using algorithms for K_C not dependant on
576 knowledge of n_{PSII} (Schuback et al. 2015) provide a means to overcome this
577 limitation.

578 As a further test of the validity of our FRRf-based approach for estimating carbon
579 uptake, we applied the procedures described above ($ETR_{daily} \times K_C$) to estimate NPP

580 from FRRf casts deployed in 2007 winter, and subsequently compared these FRRf
581 derived NPP values with those obtained from daily ^{13}C-incubation experiments. All
582 methods were the same as for 2008-2010 cruises but with no underwater spectral
583 irradiance and/or phytoplankton absorption data was not available (so constant
584 spectral correction factor of 0.64 was applied). Even so, estimation of P^B using the
585 FRRf data alone gave good agreement with the measured ^{13}C uptake, albeit with a
586 slight underestimation under conditions of high carbon uptake (Fig. 10a). We also
587 tested this FRRf-based P^B approach for estimating daily- and depth-integrated NPP
588 for the entire dataset (2007 – 2010) (Fig. 10b). Here a strong correlation was observed
589 between estimated and measured P^B and IPP both were found, and RMSE for the P^B
590 and IPP were 12.6 mgC (mgChl-a)$^{-1}$ d^{-1} and 271.8 mgC m^{-2} d^{-1}, respectively.
591 Current satellite NPP models are still considered to perform poorly in Case-2
592 waters (Saba et al., 2011) and need to be modified or localized for specific regions,
593 which in turn is dependent upon how much data is locally available (Tripathy et al.,
594 2012); thus, our FRRf-based NPP approach may provide a major step towards this
595 currently limitation. For example, popular models such as the Vertically Generalized
596 Production Model (VGPM) locally require algorithms that can improve upon the
597 generally applied optimal rate of productivity (i.e. P^B_{opt}) (Kameda and Ishizaka, 2005)
598 and thus definitely benefit from the high data volume afforded through FRRf. Thus,
599 whilst our present study has provided a first look at an improved FRRf method for
600 estimating NPP in a eutrophic embayment, we suggest that it lays the foundation for a
601 broader scale complementary approach to yield carbon-based NPP measurements for
602 further satellite model validation and/or improvement.
603
604

Acknowledgements

We wish to thank the captain, officers and crew of T/V-Kakuyo maru for their admirable assistance during onboard sampling and monuments. We also thank Dr. W. Cheah, Dr. JI. Goes, Dr. H do R. Gomes and two reviewers for helping to improve this manuscript. This research was supported by the Global Observation Mission-Climate (GCOM-C) Project of Japan Aerospace Exploration Agency. The contribution by D.J. Suggett was supported by an Australian Research Council Future Fellowship (FT130100202)

615 **Reference**
616

617 Behrenfeld MJ, Kolber ZS (1999) Widespread iron limitation of phytoplankton in the
618 South Pacific Ocean. Science 283: 840-843.
619 Behrenfeld MJ, Falkowski PG (1997) Photosynthetic rates derived from
620 satellite-based chlorophyll concentration. Limnol Oceanogr 42: 1-20.
621 Brading P, Warner ME, Smith DJ, Suggett DJ (2013) Contrasting modes of inorganic
622 carbon acquisition amongst *Symbiodinium* (Dinophyceae) phylotypes. New Phytol
623 200: 432-442.
624 Cardol P, Forti G, Finazzi G (2011) Regulation of electron transport in microalgae.
625 BBA-Bioenergetics 1807: 912-918.
626 Cheah W, McMinn A, Griffiths FB, Westwood KJ, Wright SW, et al. (2011) Assessing
627 Sub-Antarctic Zone primary productivity from fast repetition rate fluorometry.
628 Deep-Sea Res. II 58: 2179-2188.
629 Davison, I. R. 1991. Environmental Effects on algal photosynthesis: temperature. J.
630 Phycol. 27: 2-8. doi:10.1111/ j0022-3646.1991.00002.x.
631 Corno G, Letelier RM, Abbott MR, Karl DM (2006) Assessing primary production
632 variability in the north pacific subtropical gyre: a comparison of fast repetition rate
633 fluorometry and ^{14}C measurements. J Phycol 42: 51-60.
634 Debes H, Gaard E, Hansen B (2008) Primary production on the Faroe shelf: Temporal
635 variability and environmental influences. J Marine Syst 74: 686-697.
636 Fujiki T, Hosaka T, Kimoto H, Ishimaru T, Saino T (2008) In situ observation of
637 phytoplankton productivity by an underwater profiling buoy system: use of fast
638 repetition rate fluorometry. Mar Ecol Prog Ser 353: 81-88.
639 Halsey KH, O'Malley RT, Graff JR, Milligan AJ, Behrenfeld MJ (2013) A common
640 partitioning strategy for photosynthetic products in evolutionarily distinct
641 phytoplankton species. New Phytol 198: 1030-1038.
642 Hama T, Miyazaki T, Ogawa Y, Iwakuma T, Takahashi M, et al. (1983) Measurement
643 of photosynthetic production of a marine phytoplankton population using a stable
644 ^{13}C isotope. Mar Biol 73: 31-36.
645 Hancke K, Dalsgaard T, Sejr MK, Markager S, Glud RN (2015) Phytoplankton
646 Productivity in an Arctic Fjord (West Greenland): Estimating Electron
647 Requirements for Carbon Fixation and Oxygen Production. PLoS ONE 10(7):
648 e0133275. doi:10.1371/journal.pone.0133275
649 Hirawake T, Shinmyo K, Fujiwara A, Saitoh S-i (2012) Satellite remote sensing of
650 primary productivity in the Bering and Chukchi Seas using an absorption-based
651 approach. ICES J Mar Sci 69: 1194-1204.
652 Ishizaka J, Kitaura Y, Touke Y, Sasaki H, Tanaka A, et al. (2006) Satellite detection of
653 red tide in Ariake Sound, 1998–2001. J Oceanogr 62: 37-45.
654 Jassby AD, Platt T (1976) Mathematical formulation of the relationship between
655 photosynthesis and light for phytoplankton. Limnol Oceanogr 21: 540-547.
656 Kameda T, Ishizaka J (2005) Size-fractionated primary production estimated by a
657 two-phytoplankton community model applicable to ocean color remote sensing. J
658 Oceanogr 61: 663-672.
659 Kishino M, Takahashi M, Okami N, Ichimura S (1985) Estimation of the spectral
660 absorption coefficients of phytoplankton in the sea. B Mar Sci 37: 634-642.
661 Kolber ZS, Prášil O, Falkowski PG (1998) Measurements of variable chlorophyll
662 fluorescence using fast repetition rate techniques: defining methodology and
663 experimental protocols. BBA-Bioenergetics 1367: 88-106.
664 Kolber ZS, Falkowski PG (1993) Use of active fluorescence to estimate

665 phytoplankton photosynthesis in situ. Limnol Oceanogr 38: 1646-1665.
666 Kromkamp JC, Dijkman NA, Peene J, Simis SG, Gons HJ (2008) Estimating
667 phytoplankton primary production in Lake IJsselmeer (The Netherlands) using
668 variable fluorescence (PAM-FRRF) and C-uptake techniques. Eur J Phycol 43:
669 327-344.
670 Lavaud J, Rousseau B, Etienne AL (2004) General Features of Photoprotection By
671 Energy Dissipation in Planktonic Diatoms (Bacillariophyceae). J Phycol 40:
672 130-137.
673 Lawrenz E, Silsbe G, Capuzzo E, Ylöstalo P, Forster RM, et al. (2013) Predicting the
674 Electron Requirement for Carbon Fixation in Seas and Oceans. PLoS ONE 8(3):
675 e58137. doi:10.1371/journal.pone.0058137 .
676 López-Sandoval DC, Rodríguez-Ramos T, Cermeño P, Sobrino C, Marañón E (2014)
677 Photosynthesis and respiration in marine phytoplankton: Relationship with cell size,
678 taxonomic affiliation, and growth phase. J Exp Mar Biol Ecol 457: 151-159.
679 Mackey KR, Paytan A, Grossman AR, Bailey S (2008) A photosynthetic strategy for
680 coping in a high‐light, low‐nutrient environment. Limnol Oceanogr 53:
681 900-913.
682 Marra JF (2015) Ocean productivity: A personal perspective since the first Liege
683 Colloquium. J Marine Syst. 147: 3-8.
684 Marra JF (2009) Net and gross productivity: weighing in with ^{14}C. Aquat Microb Ecol
685 56: 123-131.
686 McDonald AE, Ivanov AG, Bode R, Maxwell DP, Rodermel SR, et al. (2011)
687 Flexibility in photosynthetic electron transport: the physiological role of
688 plastoquinol terminal oxidase (PTOX). BBA-Bioenergetics 1807: 954-967.
689 Melrose DC, Oviatt CA, O Reilly JE, Berman MS (2006) Comparisons of fast
690 repetition rate fluorescence estimated primary production and ^{14}C uptake by
691 phytoplankton. Mar Ecol Prog Ser 311: 37-46.
692 Mino Y, Matsumura S, Lirdwitayaprasit T, Fujiki T, Yanagi T, et al. (2014) Variations
693 in phytoplankton photo-physiology and productivity in a dynamic eutrophic
694 ecosystem: a fast repetition rate fluorometer-based study. J Plankton Res:
695 36:398-411.
696 Moore CM, Suggett DJ, Hickman AE, Kim Y-N, Tweddle JF, et al. (2006)
697 Phytoplankton photoacclimation and photoadaptation in response to environmental
698 gradients in a shelf sea. Limnol Oceanogr 51: 936-949.
699 Moore CM, Mills MM, Langlois R, Milne A, Achterberg EP, et al. (2008) Relative
700 influence of nitrogen and phosphorous availability on phytoplankton physiology
701 and productivity in the oligotrophic sub‐tropical North Atlantic Ocean. Limnol
702 Oceanogr 53: 291-305.
703 Ott T, Clarke J, Birks K, Johnson G (1999) Regulation of the photosynthetic electron
704 transport chain. Planta 209: 250-258.
705 Oxborough K, Moore CM, Suggett DJ, Lawson T, Chan HG, et al. (2012) Direct
706 estimation of functional PSII reaction center concentration and PSII electron flux
707 on a volume basis: a new approach to the analysis of Fast Repetition Rate
708 fluorometry (FRRf) data. Limnol Oceanogr: Methods 10: 142-154.
709 Prasil O, Kolber Z, Berry JA, Falkowski PG (1996) Cyclic electron flow around
710 photosystem II in vivo. Photosynth Res 48: 395-410.
711 Raateoja M, Seppälä J, Kuosa H (2004) Bio-optical modelling of primary production
712 in the SW Finnish coastal zone, Baltic Sea: fast repetition rate fluorometry in Case
713 2 waters. Mar Ecol Prog Ser 267: 9-26.
714 Robinson C, Suggett D, Cherukuru N, Ralph P, Doblin M (2014) Performance of Fast

715 Repetition Rate fluorometry based estimates of primary productivity in coastal
716 waters. J Marine Syst. 139: 299-310.
717 Saba VS, Friedrichs MAM, Antoine D, Armstrong RA, Asanuma I, et al. (2011) An
718 evaluation of ocean color model estimates of marine primary productivity in coastal
719 and pelagic regions across the globe. Biogeosciences 8: 489-503.
720 Schuback N, Schallenberg C, Duckham C, Maldonado MT, Tortell PD (2015)
721 Interacting Effects of Light and Iron Availability on the Coupling of Photosynthetic
722 Electron Transport and CO_2-Assimilation in Marine Phytoplankton. PLoS ONE
723 10(7): e0133235. doi:10.1371/journal. pone.0133235.
724 Serôdio J, Lavaud J (2011) A model for describing the light response of the
725 nonphotochemical quenching of chlorophyll fluorescence. Photosynth Res 108:
726 61-76.
727 Shibata T, Tripathy SC, Ishizaka J (2010) Phytoplankton pigment change as a
728 photoadaptive response to light variation caused by tidal cycle in Ariake Bay, Japan.
729 J Oceanogr 66: 831-843.
730 Silsbe GM, Oxborough K, Suggett DJ, Forster RM, Ihnken S, et al. (2015) Toward
731 autonomous measurements of photosynthetic electron transport rates: An evaluation
732 of active fluorescence ‐ based measurements of photochemistry. Limnol Oceanogr:
733 Methods 13: 138-155.
734 Smyth T, Pemberton K, Aiken J, Geider R (2004) A methodology to determine
735 primary production and phytoplankton photosynthetic parameters from fast
736 repetition rate fluorometry. J Plankton Res 26: 1337-1350.
737 Suggett DJ, MacIntyre HL, Kana TM, Geider RJ (2009a) Comparing electron
738 transport with gas exchange: parameterising exchange rates between alternative
739 photosynthetic currencies for eukaryotic phytoplankton. Aquat Microb Ecol 56:
740 147-162.
741 Suggett DJ, MacIntyre HL, Geider RJ (2004) Evaluation of biophysical and optical
742 determinations of light absorption by photosystem II in phytoplankton. Limnol
743 Oceanogr: Methods 2: 316-332.
744 Suggett DJ, Moore CM, Hickman AE, Geider RJ (2009b) Interpretation of fast
745 repetition rate (FRR) fluorescence: signatures of phytoplankton community
746 structure versus physiological state. Mar Ecol Prog Ser 376: 1-19.
747 Suggett DJ, Kraay G, Holligan P, Davey M, Aiken J, et al. (2001) Assessment of
748 photosynthesis in a spring cyanobacterial bloom by use of a fast repetition rate
749 fluorometer. Limnol Oceanogr 46: 802-810.
750 Suggett DJ, Goyen S, Evenhuis C, Szabó M, Pettay DT, et al. (2015) Functional
751 diversity of photobiological traits within the genus Symbiodinium appears to be
752 governed by the interaction of cell size with cladal designation. New Phytol 208:
753 370–381.
754 Suggett DJ, Moore CM, Marañón E, Omachi C, Varela RA, et al. (2006b)
755 Photosynthetic electron turnover in the tropical and subtropical Atlantic Ocean.
756 Deep-Sea Res. II: 1573-1592.
757 Suggett DJ, Maberly SC, Geider RJ (2006a) Gross photosynthesis and lake
758 community metabolism during the spring phytoplankton bloom. Limnol Oceanogr
759 51: 2064-2076.
760 Suggett DJ, Moore MC and Geider RJ (2011) Estimating Aquatic Productivity from
761 Active Fluorescence Measurements. in:Chlorophyll a fluorescence in aquatic
762 sciences: methods and applications: Springer, Chapter 6, pp: 103-115.
763 Suggett DJ, Warner ME, Smith DJ, Davey P, Hennige S, et al. (2008) Photosynthesis
764 and production of hydrogen peroxide by symbiodinium (pyrrhophyta) phylotypes

765 with different thermal tolerances. J Phycol 44: 948-956.
766 Suzuki R, Ishimaru T (1990) An improved method for the determination of
767 phytoplankton chlorophyll using N, N-dimethylformamide. J Oceanogr Soc Japan
768 46: 190-194.
769 Tabata T, Hiramatsu K, Harada M (2015) Assessment of the Water Quality in the
770 Ariake Sea Using Principal Component Analysis. J Water Resource Prot 7: 41-49.
771 Tripathy SC, Ishizaka J, Siswanto E, Shibata T, Mino Y (2012) Modification of the
772 vertically generalized production model for the turbid waters of Ariake Bay,
773 southwestern Japan. Estuar Coast Shelf S 97: 66-77.
774 Tripathy SC, Ishizaka J, Fujiki T, Shibata T, Okamura K, et al. (2010) Assessment of
775 carbon- and fluorescence-based primary productivity in Ariake Bay, southwestern
776 Japan. Estuar Coast Shelf S 87: 163-173.
777 Wang SQ, Ishizaka J, Yamaguchi H, Tripathy SC, Hayashi M, et al. (2014) Influence
778 of the Changjiang River on the light absorption properties of phytoplankton from
779 the East China Sea. Biogeosciences 11: 1759-1773.
780
781

Lists of tables

Table 1 Details of the sampling and environmental characteristics during the sampling.

No.	Sampling date	Sampling periods	Daily PAR(0^+) (mol quanta m^{-2} d^{-1})	Z_{eu} (1% surface PAR, m)	Mixed layer depth (m)
1	28 May, 2008	6:00 – 18:00	19.07	15.0	5
2	08 Nov., 2008	8:00 – 16:00	14.99	20.0	19
3	15 Nov., 2008	8:00 – 16:00	14.58	11.0	17
4	08 Nov., 2009	6:00 – 16:00	33.68	16.8	6
5	15 Nov., 2009	6:00 – 16:00	24.19	17.0	12
6	14 May, 2010	6:00 – 18:00	68.18	11.0	7
7	21 May, 2010	6:00 – 18:00	53.36	15.2	8

Table 2 Definitions of photosynthetic parameters. ([a] Referred to Suggett et al., 2006a,b)

Parameter	Definition
E	Instantaneous irradiance (μmol quanta m^{-2} s^{-1})
F_o	Minimum fluorescence yield in dark chamber (arbitrary units: a.u.)
F_m	Maximum fluorescence yield in dark chamber (a.u.)
F_v/F_m	Potential photochemical efficiency of open reaction centers [=(F_m - F_o)/ F_m] (dimensionless)
F'	Steady-state fluorescence yields in light chamber (a.u.)
F_m'	Maximum fluorescence yield in light chamber (a.u.)
F_q'/F_m'	Photochemical efficiency of PSII under actinic light
q_p (F_q'/F_v')	Photochemical quenching coefficient, as the difference in the apparent PSII photochemical efficiency betwe FRRf light and dark chamber quasi-simultaneously,= $[\frac{(F_m' - F')/F_m' \text{ light } chamber}{(F_m - F_o)/F_m \text{ dark } chamber}]$[a], (dimensionless)
n_{PSII}	Photosynthetic unit size of PSII (=0.002) (mol RCII (mol Chla)$^{-1}$)
σ_{PSII}	Effective absorption cross section of PSII in dark chamber (Å^2 quanta^{-1})
σ_{PSII}'	Effective absorption cross section of PSII in light chamber (Å^2 quanta^{-1})
σ_{PSII}^{abs}	Spectral corrected effective absorption cross section of PSII (Å^2 quanta^{-1})
ETR	Rate of electron transport through PSII (mmol e^- (mg Chl-a)$^{-1}$ h^{-1})
K_C	Electron requirement for carbon fixation (mol e^- (mol C)$^{-1}$)

Table 3 Summary of PAR, σ_{PSII}^{abs} and q_p ranges in two example cruises

Cruise time	instantaneous PAR (surface) (μmol quanta m^{-2} s^{-1})	σ_{PSII}^{abs} (Å^2 quanta^{-1})	q_p (surface) (dimensionless)
08 Nov., 2008 (Nov.)	45.9 - 665.1	296 - 403	0.64 - 0.96
21 May, 2010 (May)	56.7 - 1321.8	248 - 386	0.50 - 0.94

Table 4 The estimated ETR-irradiance parameters for each cruise.

	May 28, 2008	Nov. 08 2008	Nov. 15 2008	Nov. 08 2009	Nov. 15 2009	May 14 2010	May 21 2010
α	0.016 (0.001)	0.015 (0.001)	0.014 (0.001)	0.012 (0.001)	0.011 (0.001)	0.011 (0.001)	0.010 (0.001)
ETR_{max}	8.42 (0.19)	7.66 (0.12)	12.11 (0.58)	11.43 (0.33)	15.64 (0.24)	10.64 (0.31)	11.06 (0.21)

Initial slope of the ETR-PAR curve (α) and the estimated maximum ETR value (ETR_{max}) with fitting standard error

Table 5 Spearman correlation coefficients for correlations between daily K_C and environmental variables

	PAR	Temp.	Salinity	Chl-a	NO_3^-+NO_2^-	PO_4^{3-}	SiO_2
K_C	0.941** n=20	-0.185 n=20	-0.200 n=20	0.065 n=20	-0.211 n=20	-0.298 n=20	-0.0484 n=20

** indicates significance of the correlation at the 0.01 significant level.

Lists of figures

Fig. 1 Location of Ariake Bay and sampling station.

Fig. 2 Representative vertical profiles **(a)** daily PAR (mol quanta m^{-2} d^{-1}); **(b)** temperature (℃). Arrows indicate Z_{eu} depth of each cruise; **(c)** salinity and **(d)** potential density from pre-dawn CTD cast of each cruise. The two profiles with solid lines were typical water characteristics in May and November; specifically cruises from 21 May 2010 and 8 November 2008.

Fig. 3 Representative vertical profiles **(a)** NO_3^-+NO_2^- (μM); **(b)** PO_4^{3-} (μM); **(c)** SiO_2 (μM), **(d)** N/P ratio (dimensionless) and **(e)** Chl-a (mg m^{-3})**.**

Fig. 4 Time series profiles of FRRf-based data σ_{PSII}^{abs} **(a, e)**, F_v/F_m **(**dimensionless**; b, f)**, q_p **(**dimensionless**; c, g)** and ETR **(**mmol e^- [mgChl-a]$^{-1}$ h^{-1}; **d, h)**. Upper and lower panels are for cruise data of 21 May 2010 (a-d) and 8 November 2008 (e-h)

Fig.5 Vertical profiles of the σ_{PSII} correction factor (dimensionless) in 21 May 2010 and 8 November 2008 cruise. Absorption data was collected from the same cast as for the water samples for ^{13}C uptake experimentation; underwater spectral irradiance was measured at local noon

Fig. 6 ETR(mmol e^- [mgChl-a]$^{-1}$ h^{-1}) – PAR(μmol quanta m^{-2} s^{-1}) fitting results for cruises on **a)** 28 May, 2008; **b)** 08 Nov., 2008; **c)** 15 Nov., 2008; **d)** 08 Nov., 2009; **e)** 15 Nov., 2009; **f)** 14 May, 2010; **g)** 21 May, 2010. Scatter data is the measured FRRf based ETRs from all time series casts and the dotted line is the model fit. Fitting statistics for each curve are summarized in Table 4.

Fig. 7 (a) Daily-integrated ETR (mmol e^- [mgChl-a]$^{-1}$ d^{-1}) profiles plotted against optical depth for each cruise; and **(b)** plots of daily-integrated ETR (mmol e^- [mgChl-a]$^{-1}$ d^{-1}) against daily-integrated PAR (mol quanta m^{-2} d^{-1}). The dotted lines are the fitted tanh function.

Fig. 8 (a) ^{13}C-uptake based determinations of Chla-specific carbon uptake **(** P^B , mgC mg Chl-a^{-1} d^{-1}) plotted against optical depth for each cruise; and **(b)** Scatter plots of P^B (mmol C [mgChl-a]$^{-1}$ d^{-1}) against corresponding measurements of daily-integrated ETR (mmol e^- [mgChl-a]$^{-1}$ d^{-1}). Dotted line represents where ETR is 20 mmol e^- [mgChl-a]$^{-1}$ d^{-1}, i.e the point at which the linear correlation between ETR and P^B appears to break down.

Fig. 9 Profiles of **(a)** all K_C values (mol e^- (mol C)$^{-1}$) and **(b)** excluding data where K_C < 4 mol e^- (mol C)$^{-1}$; **(c,d)** Scatter plot of the relationship between K_C versus daily PAR (mol quanta m^{-2} d^{-1}) and NPQ Proxy (dimensionless). The linear equations are the results from Type II regression.

Fig. 10 (a) Comparisons of measured Chla-specific ^{13}C-uptake rates against estimated from FRRf- based ETRs obtained in 2007 and K_C model (Fig. 9(c)) and **(b)** measured depth-integrated primary productivities against FRRf-based estimated for all cruises across 2007 – 2010.

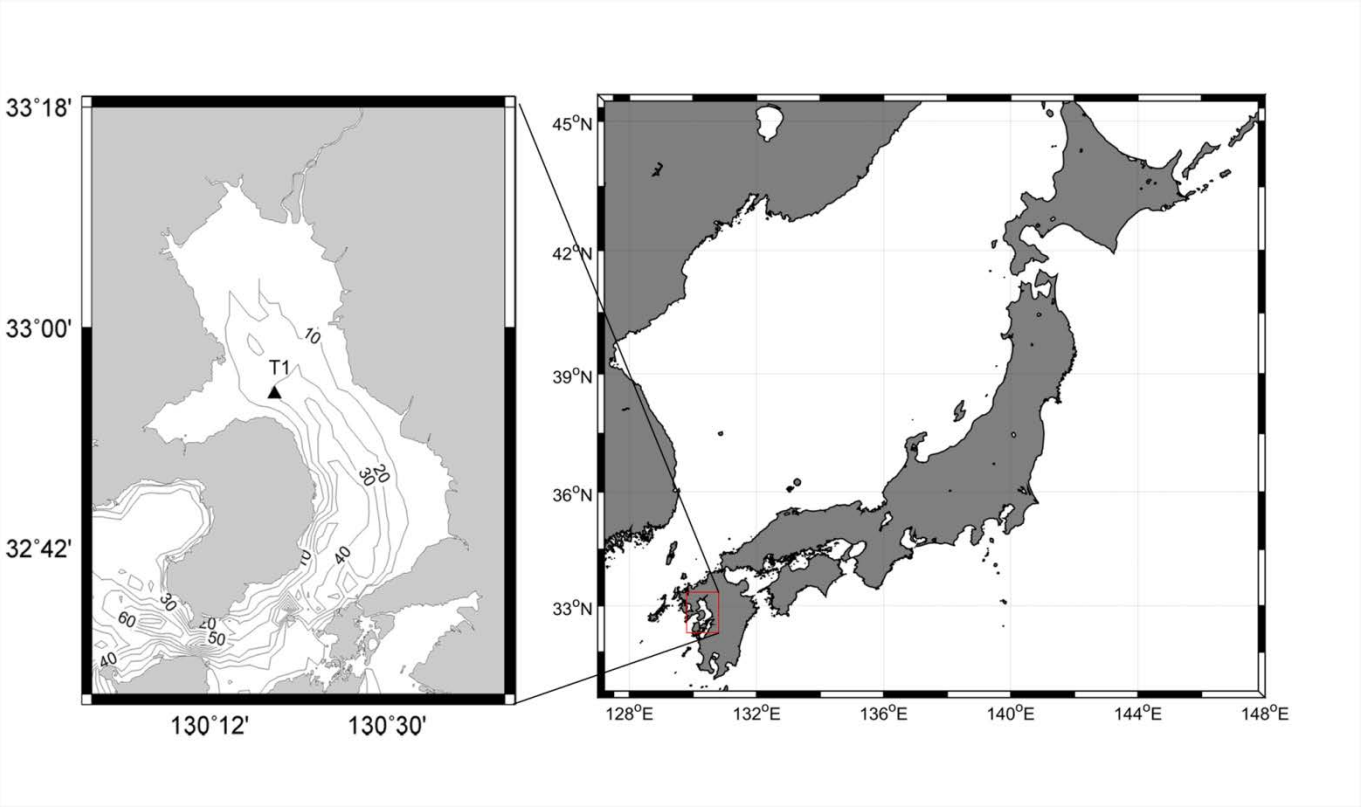
33°18'
33°00'
32°42'
130°12'
130°30'
T1
10
20
30
40
50
60
45°N
42°N
39°N
36°N
33°N
128°E
132°E
136°E
140°E
144°E
148°E

Fig. 1

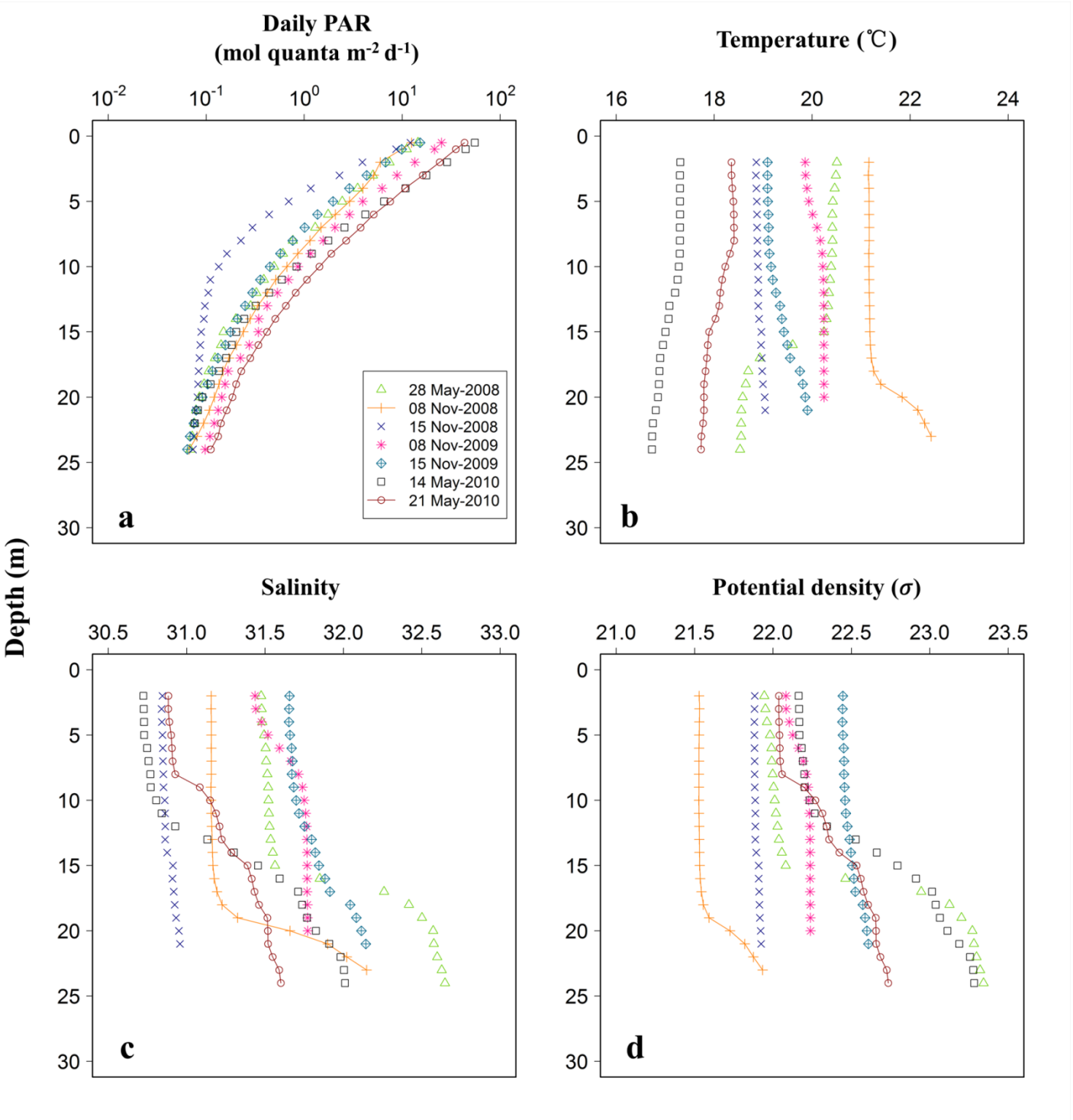
Daily PAR
(mol quanta m-2 d-1)
Temperature (℃)
Salinity
Potential density (σ)
Depth (m)
28 May-2008
08 Nov-2008
15 Nov-2008
08 Nov-2009
15 Nov-2009
14 May-2010
21 May-2010
a
b
c
d

Fig. 2

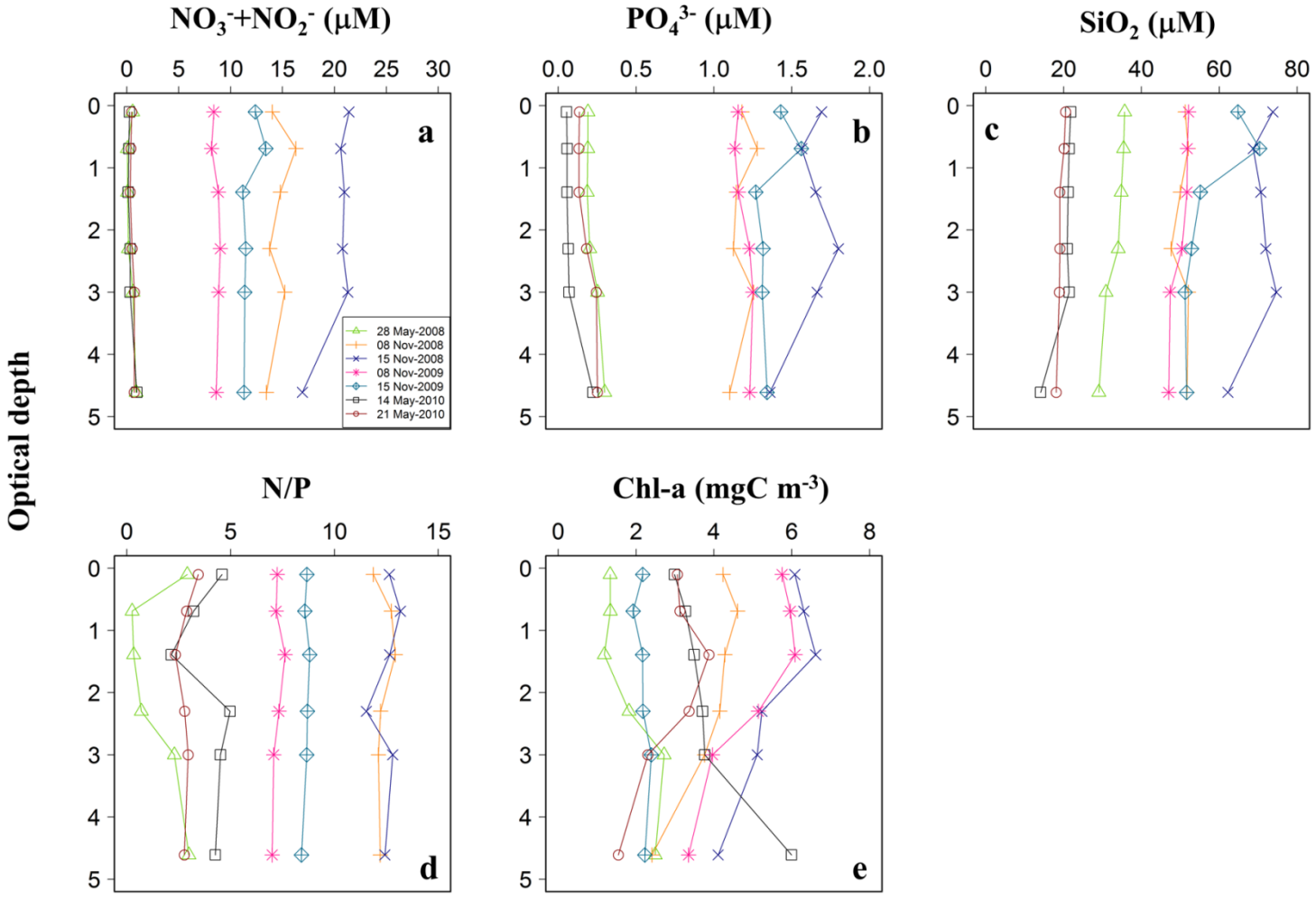
Optical depth
NO3-+NO2- (µM)
PO43- (µM)
SiO2 (µM)
N/P
Chl-a (mgC m-3)
a
b
c
d
e
28 May-2008
08 Nov-2008
15 Nov-2008
08 Nov-2009
15 Nov-2009
14 May-2010
21 May-2010

Fig. 3

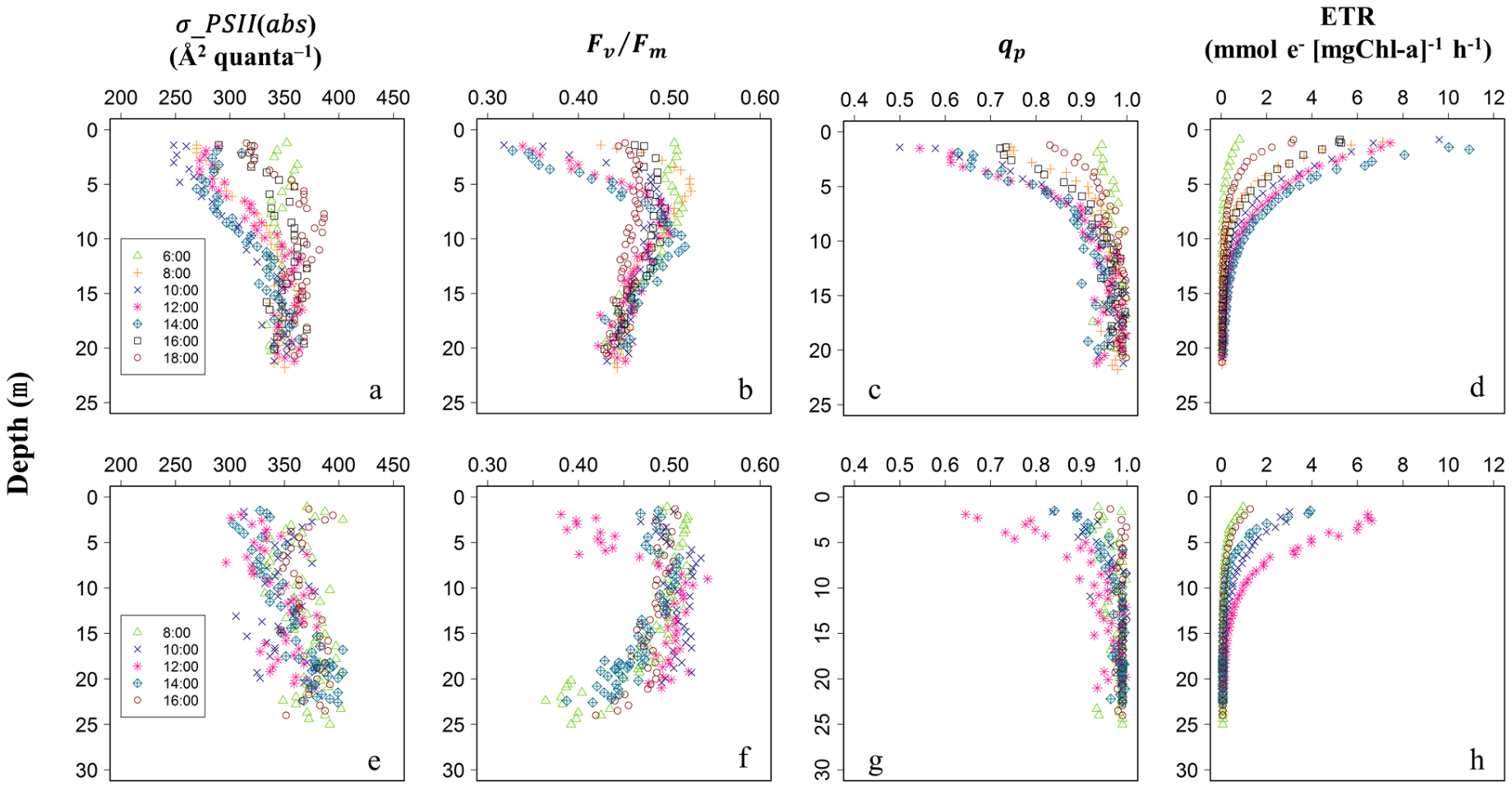
σ_PSII(abs)
(Å² quanta⁻¹)
Fv/Fm
qp
ETR
(mmol e⁻ [mgChl-a]⁻¹ h⁻¹)
Depth (m)
6:00
8:00
10:00
12:00
14:00
16:00
18:00
a
b
c
d
e
f
g
h

Fig. 4

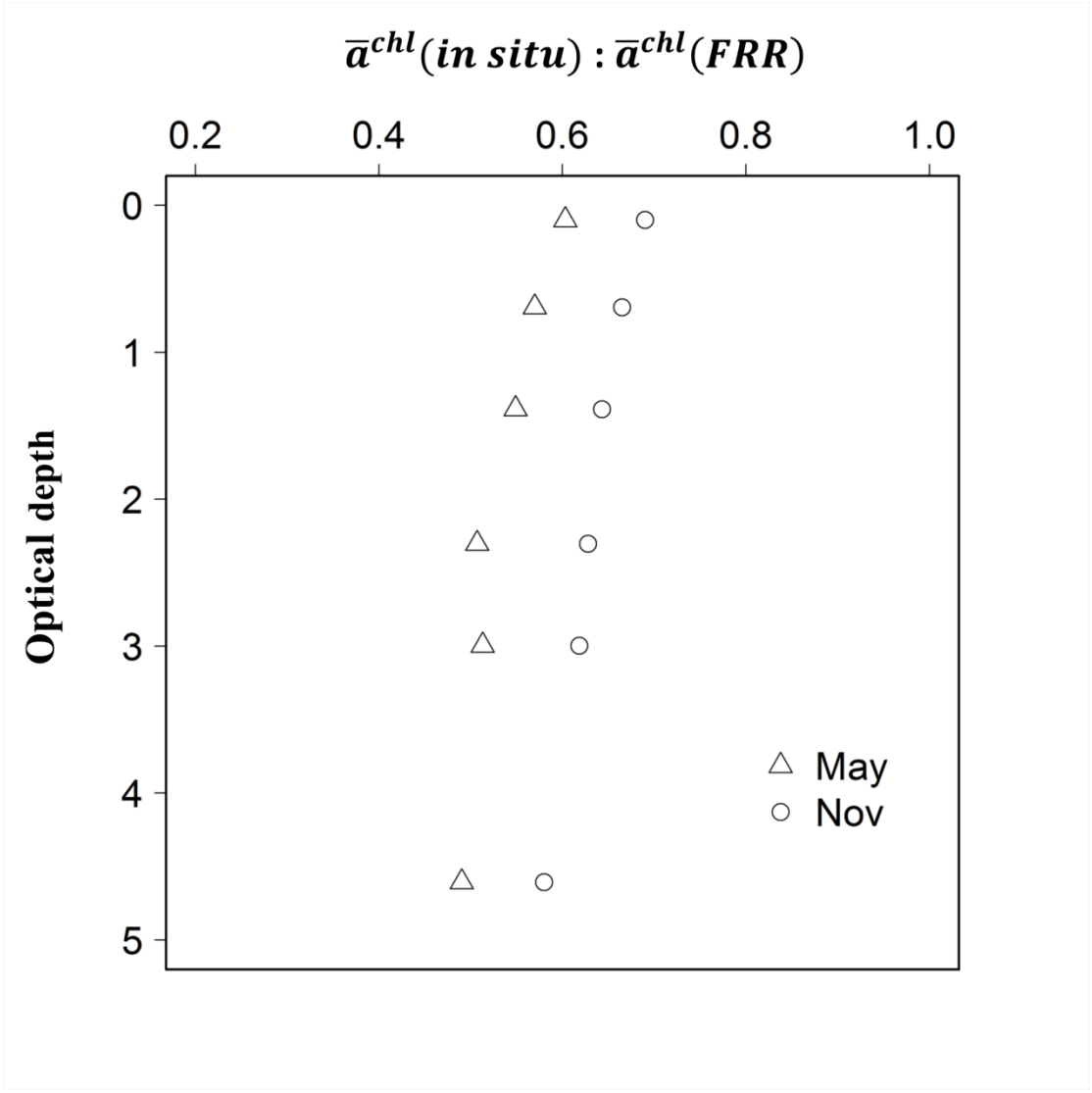
$\overline{a}^{chl}(in\ situ) : \overline{a}^{chl}(FRR)$
0.2
0.4
0.6
0.8
1.0
0
1
2
3
4
5
Optical depth
May
Nov

Fig. 5

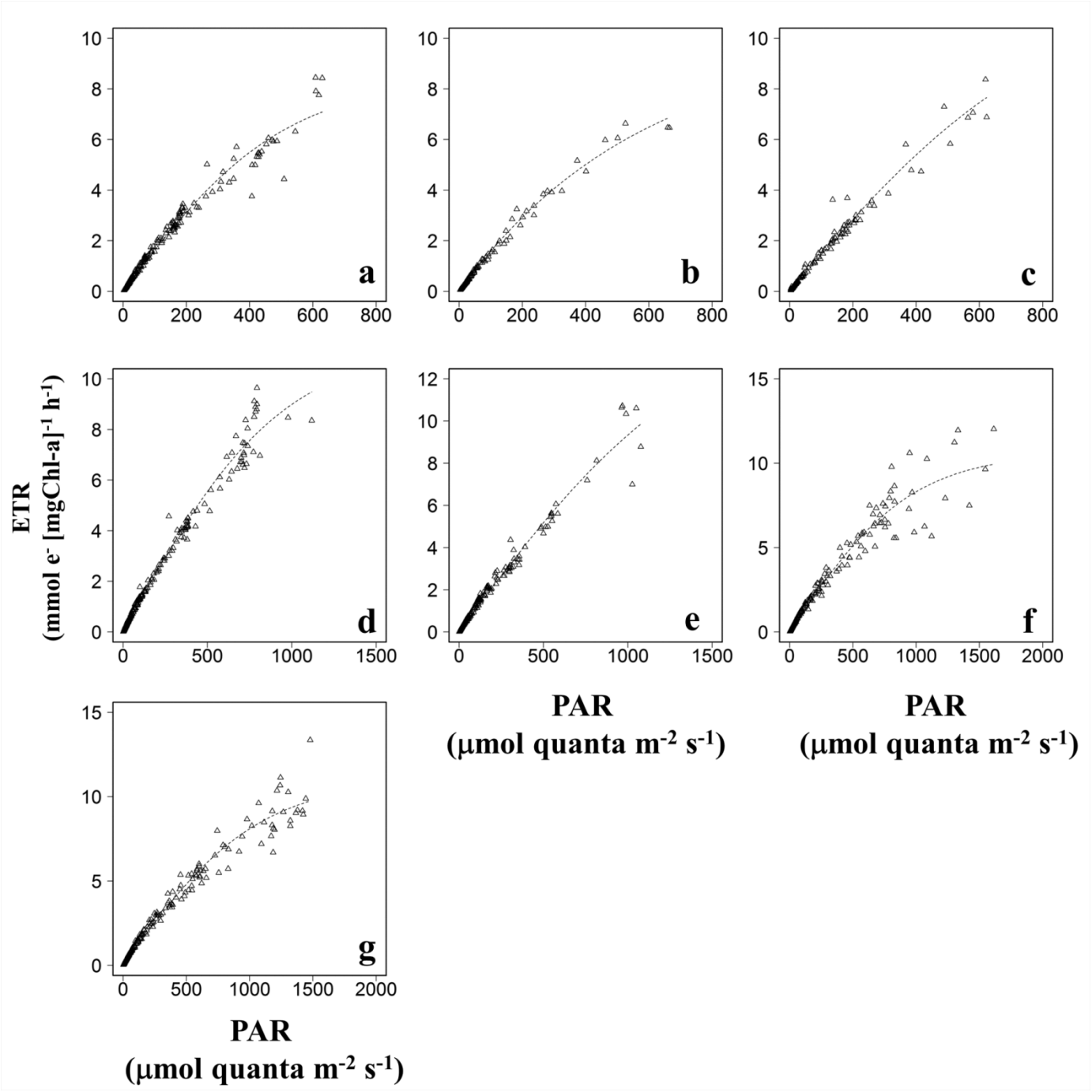
a
b
c
d
e
f
g
ETR
(mmol e- [mgChl-a]-1 h-1)
PAR
(µmol quanta m-2 s-1)
PAR
(µmol quanta m-2 s-1)
PAR
(µmol quanta m-2 s-1)

Fig. 6

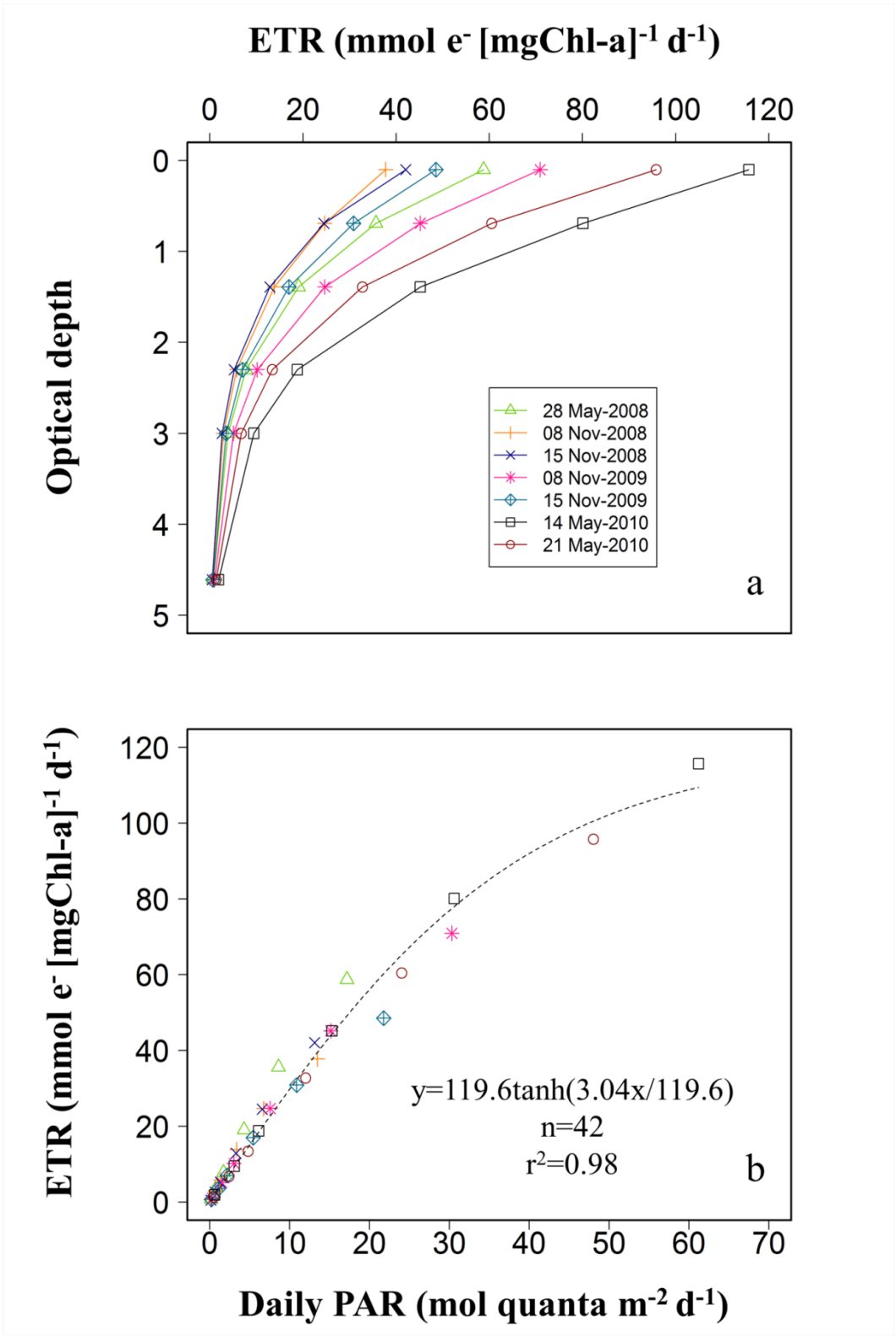
ETR (mmol e- [mgChl-a]-1 d-1)
Optical depth
28 May-2008
08 Nov-2008
15 Nov-2008
08 Nov-2009
15 Nov-2009
14 May-2010
21 May-2010
a
ETR (mmol e- [mgChl-a]-1 d-1)
y=119.6tanh(3.04x/119.6)
n=42
r2=0.98
b
Daily PAR (mol quanta m-2 d-1)

Fig. 7

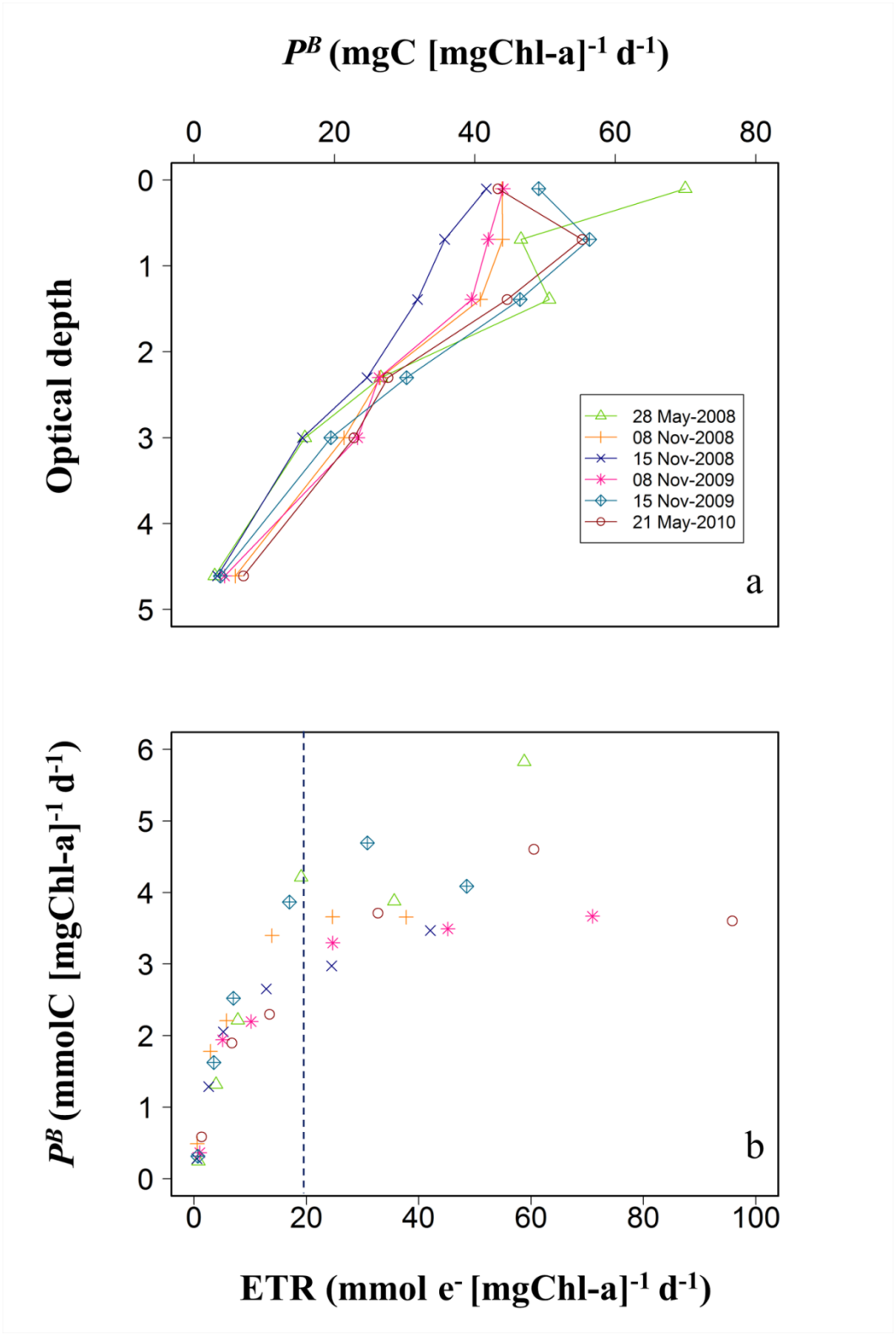
P^B (mgC [mgChl-a]$^{-1}$ d^{-1})
Optical depth
28 May-2008
08 Nov-2008
15 Nov-2008
08 Nov-2009
15 Nov-2009
21 May-2010
a
P^B (mmolC [mgChl-a]$^{-1}$ d^{-1})
b
ETR (mmol e$^-$ [mgChl-a]$^{-1}$ d^{-1})

Fig. 8

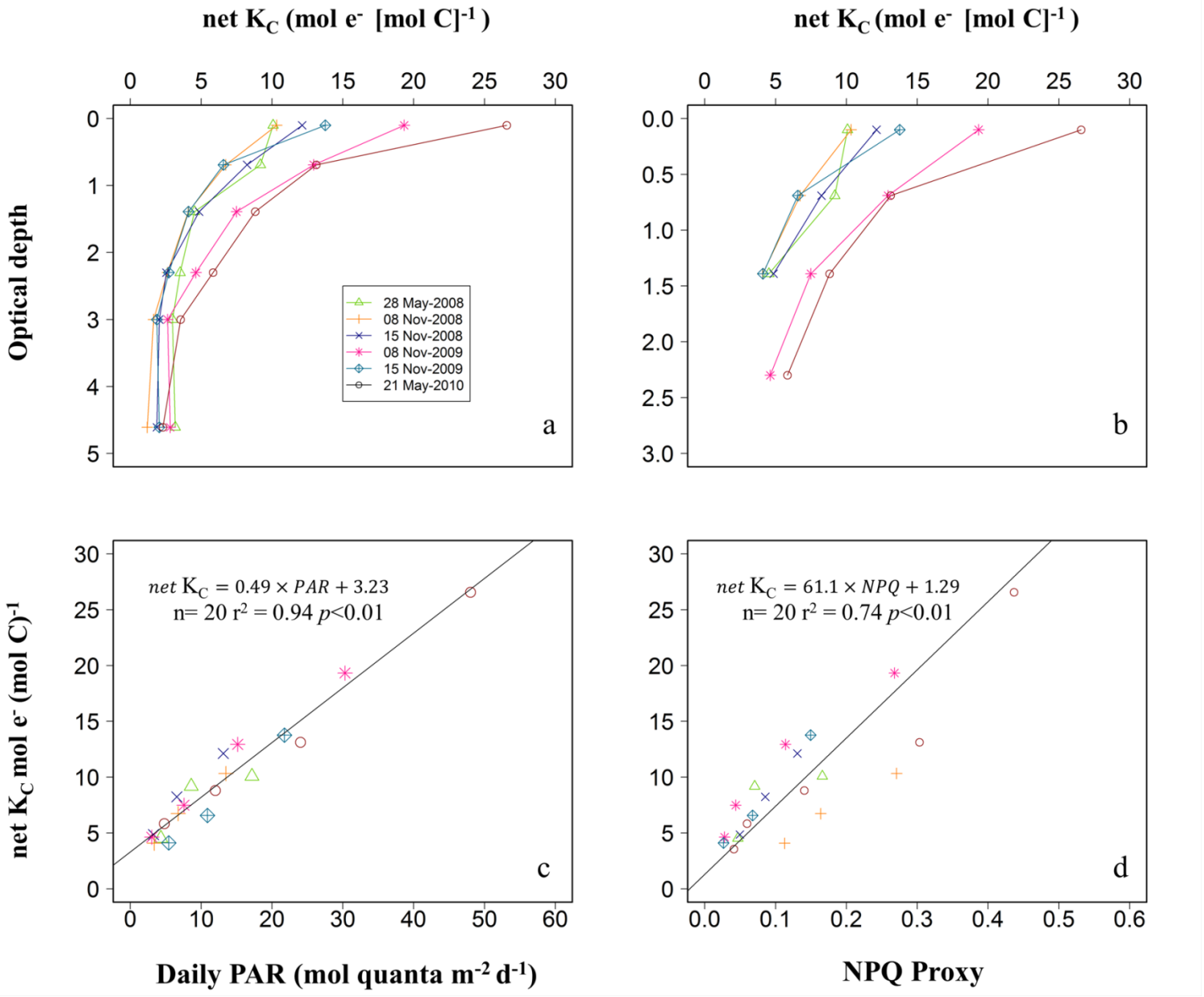
net K_C (mol e^- [mol C]$^{-1}$)
Optical depth
28 May-2008
08 Nov-2008
15 Nov-2008
08 Nov-2009
15 Nov-2009
21 May-2010
a
b
net K_C mol e^- (mol C)$^{-1}$
$net\ K_C = 0.49 \times PAR + 3.23$
n= 20 r^2 = 0.94 p<0.01
c
$net\ K_C = 61.1 \times NPQ + 1.29$
n= 20 r^2 = 0.74 p<0.01
d
Daily PAR (mol quanta m^{-2} d^{-1})
NPQ Proxy

Fig. 9

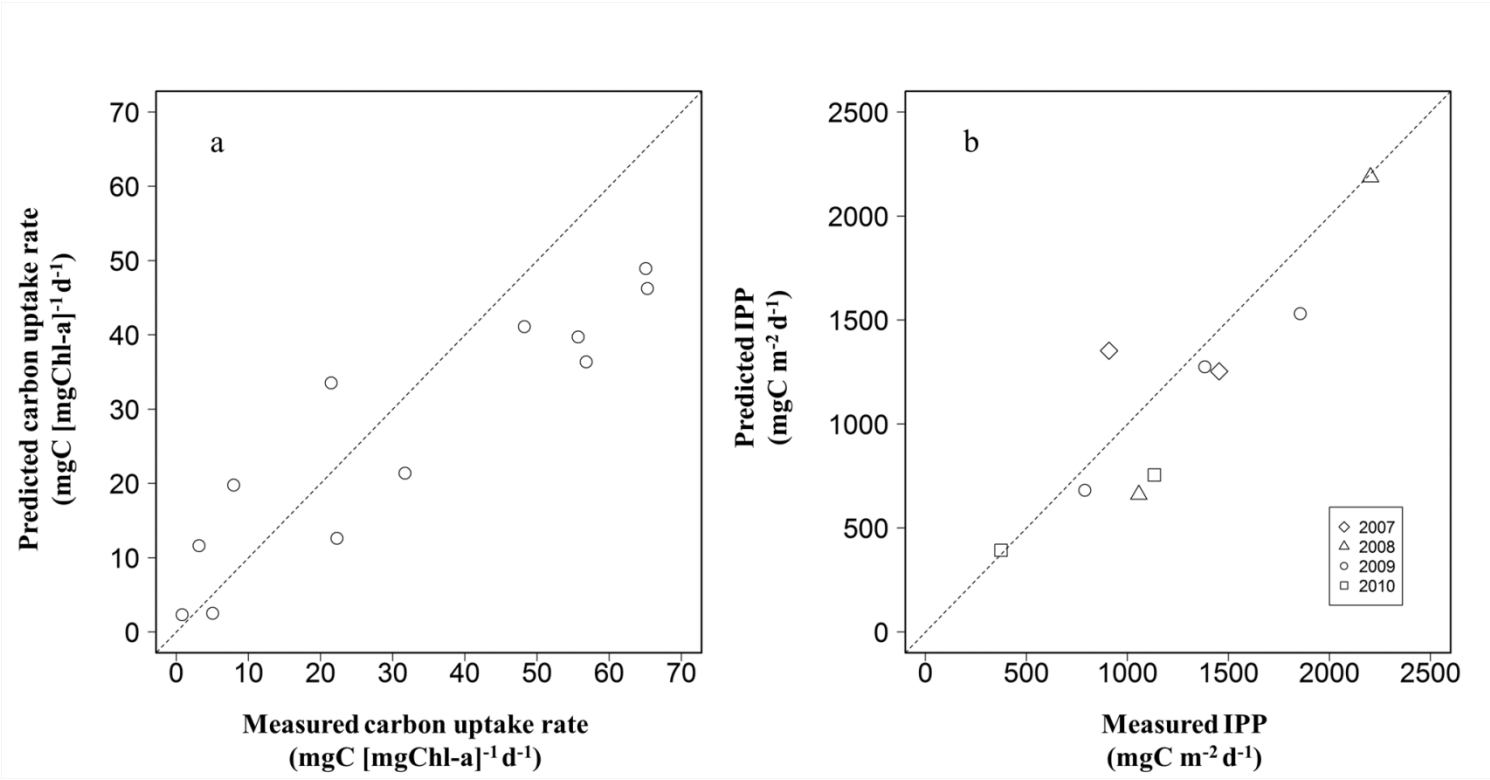
a
Predicted carbon uptake rate
(mgC [mgChl-a]-1 d-1)
Measured carbon uptake rate
(mgC [mgChl-a]-1 d-1)
0
10
20
30
40
50
60
70
b
Predicted IPP
(mgC m-2 d-1)
Measured IPP
(mgC m-2 d-1)
0
500
1000
1500
2000
2500
2007
2008
2009
2010

Fig. 10